Lawrence Berkeley National Laboratory
Recent Work

Title
SUCCESSFUL MOLECULAR BEAM EPITAXY GROWTH AND CHARACTERIZATION OF (110) GaAs/GaAs AND (110) AlGaAs/GaAs

Permalink
https://escholarship.org/uc/item/3zj3c39s

Author
Allen, L.P.

Publication Date
1987-03-01

eScholarship.org Powered by the California Digital Library
University of California

LBL-23427
c.2

Lawrence Berkeley Laboratory

UNIVERSITY OF CALIFORNIA

Materials & Chemical Sciences Division

JUN 26 1987

SUCCESSFUL MOLECULAR BEAM EPITAXY GROWTH AND CHARACTERIZATION OF (110) GaAs/GaAs and (110) AlGaAs/GaAs

Lisa Parechanian Allen
(Ph.D. Thesis)

March 1987

TWO-WEEK LOAN COPY
This is a Library Circulating Copy
which may be borrowed for two weeks.

Prepared for the U.S. Department of Energy under Contract DE-AC03-76SF00098

LBL-23427 c.2

DISCLAIMER

This document was prepared as an account of work sponsored by the United States Government. While this document is believed to contain correct information, neither the United States Government nor any agency thereof, nor the Regents of the University of California, nor any of their employees, makes any warranty, express or implied, or assumes any legal responsibility for the accuracy, completeness, or usefulness of any information, apparatus, product, or process disclosed, or represents that its use would not infringe privately owned rights. Reference herein to any specific commercial product, process, or service by its trade name, trademark, manufacturer, or otherwise, does not necessarily constitute or imply its endorsement, recommendation, or favoring by the United States Government or any agency thereof, or the Regents of the University of California. The views and opinions of authors expressed herein do not necessarily state or reflect those of the United States Government or any agency thereof or the Regents of the University of California.

SUCCESSFUL MOLECULAR BEAM EPITAXY GROWTH AND CHARACTERIZATION OF (110) GaAs/GaAs AND (110) AlGaAs/GaAs

Lisa Parechanian Allen

Department of Materials Science and Mineral Engineering
University of California
and
Materials and Chemical Sciences Division
Lawrence Berkeley Laboratory
University of California
Berkeley, CA 94720

This work was supported by the Materials Science Division of the U.S. Department of Energy under Contract No. DE-AC03-76SF00098.

DEDICATION

The adventure of a student in obtaining a Ph.D. has a great deal to do with the outlook on life that the student develops. For this student, life in graduate school was suddenly wonderful after meeting my husband, Scott. In addition, I had the good fortune to work with a brilliant professor, Eicke Weber, and to come to know and value the profound wisdom and years of top notch research by Professor Jack Washburn. I am also quite grateful to a very special mentor, Dr. Zusanna Liliental-Weber. With the support of my husband, my parents, and my professors, my path on the road of research was, indeed, a promising one.

Writing a dedication to this thesis is somehow very fulfilling. The work is at a stopping point, and there are new adventures that I can glimpse at in the near future. Before I leave, however, I wish to heartily thank all my friends whose sense of humor and good will were so essential in the circuitous route of this journey. So, thank you Lori Madajian and J.J. Hoyt and Mark Hoinkis and Boyd Clark and Darrel Frear and Kevin Jones and Etienne Colas and Ekrem Yener and Ron Read and Pete Wilson and Joyce Olsen and Chris Cole and Lee Weinstein and Evelyn Jacobson and Sherman Chan and Lindas Calvin and Seltzer and Rosa Centenaro and Rsue Caron and Bob Smith and Mark Juanitas. Travelling with you and sharing so many events in the last few years has made life richer than any stock option could ever promise. I sincerely hope that we may continue to fraternize, play softball, and have a lot of fun together - even if it means we have to travel all over the world to conferences.

Finally, Scott and I continue to ask God for guidance so that we may be ever mindful of the needs of others and to fulfill God's plans for us in all paths of life.

TABLE OF CONTENTS

	Page
Abstract	vii
Acknowledgements	ix
List of Figures	xi
I. Introduction	1
II. Experimental	8
III. Optimal Growth Conditions for (110) GaAs as Compared to (100) GaAs	14
IV. The Nature of (110) GaAs Faceting	28
V. Examination of Initial Facet Formation and Effect of Substrate Angling	49
VI. Electrical and Optical Characteristics of Successful (110) GaAs/GaAs	63
VII. Kinetic Theory of Facet Formation and Elimination on (110) GaAs	73
VIII. Conclusion	79
Appendix I: SEM Tilting Formula	82
Appendix II: TEM Plan-View and Cross Section Technique	84
Appendix III: GaAs Lithography Process	85
Appendix IV: FCC (110) Stereographic Projection	86
References	87

SUCCESSFUL MOLECULAR BEAM EPITAXY GROWTH AND CHARACTERIZATION OF (110) GaAs/GaAs AND (110) AlGaAs/GaAs

Lisa Parechanian Allen

Department of Materials Science and Mineral Engineering
University of California
and
Materials and Chemical Sciences Division
Lawrence Berkeley Laboratory
University of California
Berkeley, CA 94720

ABSTRACT

Commonly observed faceting of (110) GaAs films grown by molecular beam epitaxy (MBE) has been analyzed. Facets were studied with respect to MBE growth parameters, the GaAs crystallography, their chemical, electrical, and optical nature, and the kinetics of initial formation. Facets were found to align along the [001] with side planes of (100) and (010). The back planes of the facets were consistently of $(11\bar{1})$Ga in nature. The facets were composed of stoichiometric GaAs but resulting films were of poor optical and electrical quality. By exposing an abundance of Ga ledges on the substrate surface, the faceting of the MBE (110) GaAs surface was eliminated. This systematic approach has, for the first time, allowed facet free epitaxy growth of (110) GaAs and (110) AlGaAs/GaAs superlattices. Facet free MBE films were examined by Hall effect, photoluminescence, deep level transient spectroscopy, and transmission electron microscopy. A model of (110) GaAs facet initiation, development, and elimination is presented.

ACKNOWLEDGEMENTS

The guidance of Professors Eicke Weber and Jack Washburn is very much appreciated. The valuable discussions and experimental proficiency of Dr. Zusanna Liliental-Weber are appreciated, as well. Helpful talks with Drs. Robert Street, Wladick Walukiewicz, Andrew Glaeser, Ron Gronsky, Douglas Collins, Tom DeVine, and Robert Hull are also gratefully acknowledged.

This thesis was supported by the Materials Science Division of the U.S. Department of Energy under contract No. DE-AC03-76SF00098.

LIST OF FIGURES

Figure 1: Optical Nomarski images of (110) GaAs epitaxy for T_s= (a) 590°C, (b) 570°C, (c) 550°C, and (d) 510°C. As/Ga=8/1 and growth rate is 1.4 microns/hr.

Table I: Hall effect data for all growth parameter variations on (110) and (100) GaAs epitaxy.

Figure 2: Optical Nomarski photographs of (110) GaAs epitaxy for T_s= (a) 570°C and (b) 550°C each with an increased As overpressure of As/Ga~12-16/1. The growth rate was 1.4 microns/hr.

Figure 3: Optical Nomarski photographs of (110) GaAs epitaxy for T_s= 570°C, As/Ga=8/1 and growth rates of (a) 0.7 microns/hr and (b) 0.35 microns/hr.

Figure 4: Optical Nomarski photograph of (110) GaAs epitaxy with combined parameters of T_s=570°C, As/Ga~12/1 and growth rate of 0.35 microns/hr.

Figure 5: Temperature dependent Hall effect of (110) GaAs vs. (100) GaAs grown with the optimal growth parameters of T_s=570°C, As/Ga~12/1, and growth rate of 1.4 microns/hr.

Figure 6: PL data for varied MBE growth parameters of both (110) and (100) GaAs epitaxy. (a) shows substrate temperature variation effect on luminescence, (b) shows increased As flux effect on luminescence, (c) shows decreased growth rate effect of luminescence, and (d) shows PL influence of the combination of optimal (110) growth parameters.

Figure 7: SEM images of (110) GaAs facets aligned along [001]: (a) (110) GaAs surface overview showing facets in various growth stages, (b) shows close-up of facet with tip, and (c) shows a side view of the facets.

Figure 8: SEM image of latex chain resting on (110) GaAs facet, showing hillock nature of facets.

Figure 9: Two-beam images of a typical facet in plan-view, confirming orientation of facets in Figure 7.

Figure 10: Microdiffraction of typical facet in plan-view with associated bright field micrograph. Full diffraction pattern shows streaking along <111> which is perpendicular to the twinning habit plane. The extra spots in the diffraction pattern indicate a twinned structure along the (111).

Figure 11: Tilting experiments in the SEM showed the back facet plane to be of $\{111\}$ and the side planes to be of $\{100\}$. Tilting was from 0° to 50° of (a) back facet planes and (b) side facet planes.

Figure 12: High resolution electron microscopy image of facet tip of plan-view sample.

Figure 13a: Ga (A-side) and As (B-side) $\{111\}$ references after distinctive etching experiment. The diffraction patterns obtained were used as a reference in the CBED experiments which determined Ga or As planes in the facets and in later experiments of substrate ledges.

Figure 13b: Full CBED diffraction patterns associated with the etched surfaces of 13a. Note the opposite configuration of the +200 and -200 disc images.

Figure 14: GaAs cross-sectional samples with respective diffraction patterns in the (011) orientation for As faces together.

Figure 15: CBED of faceted (110) GaAs plan-view sample showing that nature of the exposed back plane is Ga-rich.

Figure 16: Complete picture of facet geometry and chemical nature with respect to (110) FCC reference stereographic projection.

Figure 17: High resolution AUGER microscopy data of typical (110) GaAs facet. Inset shows simultaneous SEM image of facet examined. The spectrum compares the substrate chemical composition with that of the facet for point 2. Points 1 and 3 yielded nearly identical information as the mid-facet point 2.

Figure 18: SEM images of 100Å (top), 700Å (middle), and 1500Å (bottom) growths of (110) GaAs at 2600X (left) and 26,00X (right).

Figure 19: Reference stereographic projection showing 6° tilting directions towards (a) (010), (b) (100), (c) (111)As and (d) $(11\bar{1})$Ga. Tilting towards these planes provides different chemical natures to the ledges exposed.

Figure 20: Schematic of different ledge types exposed with tilting (110) substrate 6° toward (111)As, $(11\bar{1})$Ga and $\{100\}$. Tilting towards $\{100\}$ provides substrate ledges of

non-polar nature as shown in the cross-section, while tilting towards {111} yields ledges of all Ga or all As.

Figure 21: SEM images of 100Å (top), 700Å (middle) and 1500Å (bottom) growths of GaAs on substrate angled 6° towards (010).

Figure 22: SEM images of 100Å (top), 700Å (middle) and 2500Å (bottom) growths of GaAS on substrate angled 6° towards (100).

Figure 23: SEM images of 100Å (top), 700Å (middle) and 1500Å (bottom) growths of GaAs on substrate angled 6° towards (111)As.

Figure 24: SEM images of 100Å (top), 700Å (middle) and 1500Å (bottom) growths of GaAs on substrate angled 6° towards ($11\bar{1}$)Ga.

Figure 25: SEM image of successful one micron growth of GaAs grown on substrate angled 6° towards (111)Ga.

Figure 26: TEM images of plan-view samples of one micron growths of faceted and non-faceted (110) GaAs. Only bend contours and no defects are visible on the non-faceted (110) GaAs.

Figure 27: Variable temperature Hall effect of (110) faceted epitaxy, (110) non-faceted (angled 6° towards (111)Ga) epitaxy, and (100) GaAs standard epitaxy.

Figure 28: Variable temperature Hall mobility of the same samples as Figure 30.

Figure 29: PL data for the (110) faceted GaAs epitaxy, the (110) non-faceted (substrate angled 6° towards ($11\bar{1}$)Ga) epitaxy, the (100) GaAs standard epitaxy, and the (110) GaAs substrate.

Figure 30: Current-Voltage (IV) characteristics (left) and CV information yielding doping as a function of distance

(right) for the (110) non-faceted GaAs epitaxy (top graphs) and (100) GaAs standard (bottom graphs) epitaxy.

Table II: DLTS information of deep level concentration and peak emission temperature for (100) and non-faceted (110) GaAs epitaxy.

Figure 31: Superlattice structure of (110) MBE GaAs-AlGaAs/GaAs films.

Figure 32: Ga-As pair properly chemisorbed on the (110) GaAs surface. The configuration naturally exposes both types of {111} to the incoming molecular species. The planes are indicated by the dotted outlines.

I. INTRODUCTION

Molecular beam epitaxy (MBE) is a well established, ultra-high vacuum technique of Si and compound semiconductor crystal growth which is known for its excellent quality of epitaxy and precise dopant profile control [1,2]. GaAs grown by MBE has, in tradition with Si wafer processing, been oriented in (100) to take advantage of the natural cleavage planes normal to that crystal face, the high quality epitaxy obtained with a wide range of growth conditions, and the superb device behavior obtained with that growth direction. The (110) non-polar orientation of GaAs has been well studied in ultra high vacuum by surface scientists for its reconstruction and bonding properties [3,4]. There is a need, however, for (110) epitaxial GaAs as is indicated in published research efforts which utilize liquid phase epitaxy (LPE) or vapor phase epitaxy (VPE) as successful methods for (110) GaAs growth. The latter is an orientation virtually neglected for MBE growth. A successful effort of MBE (110) GaAs would provide an opportunity to achieve improved device behavior over other epitaxy methods and a versatile epitaxy method for alternate materials growth in this orientation.

The (110) orientation has recently been of interest for several important GaAs semiconductor applications. For example, in the area pertaining to avalanche behavior, there is a well documented experimental orientation dependence of electron and hole impact ionization rates in GaAs [5-8]. The experiments examine the dependence of impact ionization upon the threshold states along the crystal axis with

respect to the orientation of the electric field. The results show that, unlike the <100> direction, electron ionization rates are slightly higher than hole ionization rates for all values of electric field in the <110> direction. The greatest difference between the measured electron ionization rates in <100> and <110> GaAs occurs with an electric field slightly below saturation in the $(3.3\text{–}4.5) \times 10^5$ V/cm^2 range. One theory states that the conservation of energy and momentum for the process dictates that a tunneling mechanism for the (100) conduction band electrons is required, but the avalanche process is a direct one for the (110) conduction band electrons. Only in the <110> direction does there exist a threshold energy which electrons can, in theory, reach without scattering. The theory of this phenomenon is still a matter of controversy [8], but the experimental data is not in question.

Another advantage of the (110) orientation involves the area of integrated optics. McKenna and Reinhart have shown that a LPE (110) GaAs/AlGaAs modulator and polarizer can be efficiently fabricated [9]. In most double-heterostructure dielectric waveguide modulators, the internal electric field of the p-n junction is oriented parallel to either the [111] or [100] crystal axis of the material. These orientations provide only pure phase modulation because of the fact that two principal axes of the index ellipsoid, [100] and [010], are coplanar with the waveguide layer. In the case of the internal electric field aligned along [110], one axis of the index ellipsoid is in the plane of the waveguide layer while the other two axes are at 45°

to this plane. Thus, in addition to a phase modulation, the electro-optic effect also rotates the plane of polarization. Providing a further advantage in integrated optics, the researchers showed that it was possible to directly couple TE modes to TM modes in the [110] polarizer/modulator. From analogous theory, more efficient p-n junction diode modulators of GaP were fabricated when E_j was parallel to the [110] direction [10].

The recent interest of MBE growth of heterostructures such as GaAs/Si has made non-polar (110) GaAs growth a viable candidate to eliminate the sheet charge resulting from GaAs/Si growth on the polar (100) surface [11]. This appreciable sheet charge is expected to be built into the substrate/epitaxy interface as a result of growth by the polar (100) Ga or As initial layer. Even in the absence of Si diffusion into the GaAs epitaxy, the lack of electrical neutrality must be considered when forming device structures. Earlier work of the GaAs/Ge heterostructure MBE growth, ideal because of the near perfect matching of thermal expansion coefficients and comparable lattice constants, showed that a planar MBE growth of GaAs on Ge could be achieved only on the (110) surface. While all growths of Ge on GaAs were planar, only GaAs MBE on (110) Ge provided the non-polar interface resulting in successful GaAs epitaxy under the condition that that the Ga/As ratio was not far from unity [12,13]. The CLEFT process (cleavage of lateral epitaxial films for transfer) relies on the (110) orientation of GaAs to grow GaAs epitaxy which can utilize the (110) cleavage plane [14]. The films are cleaved from reusable

substrates, greatly reducing the cost of single crystal GaAs solar cells. The savings could also be applied to other GaAs devices which utilize only a thin epitaxy while supported on a thick GaAs substrate.

Finally, Schottky barrier GaAs field effect transistors fabricated on Czochralski (LEC) material have taken advantage of orientation dependent dopant diffusion [15]. Research has shown that devices fabricated with n^+ source and drain implants subjected to high temperature and stress conditions are best oriented in the [110] direction due to the minimized impurity diffusion. No device or superlattice structures have been grown by MBE on the (110) orientation and examination of these structures offer an exciting new scientific frontier.

Previous to this successful MBE (110) GaAs growth, all published MBE (110) GaAs/GaAs growths have shown highly defective surfaces with poor optical and electrical device behavior [16-18]. Ballingall and Wood studied dopant incorporation characteristics of low index orientations of GaAs and found that the epitaxial behavior of the (110) face changed from n-type to p-type above a growth temperature of 550°C. The highly faceted surface was combined with a low electron mobility of ~3000 cm^2/V-sec. Wang et al. reported a more comprehensive study of (110) GaAs that showed metal droplet formation during growth as indicated by reflective high energy electron diffraction. When As pressure was increased, the droplets ceased but the faceting remained. Under high As flux, the (110)GaAs epitaxy exhibited n-type behavior. Photoluminescence (PL) showed a low exciton peak, consistent with poor electron mobility of ~2500 cm^2/V-sec. The study showed no

V/III ratio increase that yielded a stable (110) GaAs growth and he suggested that the (211)B surface would perhaps yield a stoichiometric epitaxy surface. Wang was the first to note that the surface features were, indeed, facets.

This thesis represents the first systematic investigation of (110) GaAs/GaAs grown by MBE. Until this undertaking, the general consensus was that (110) MBE GaAs could not be grown with smooth morphology or repeatable doping behavior. Industry had not solved this problem of facet elimination on (110) GaAs, although materials science investigations had been successful in solving faceting problems in metallic FCC systems [19,20]. Thermodynamic approaches suggest that the equilibrium shapes of these systems may be polyhedral when surface transport rates become appreciable or when the surfaces of certain orientations like (110) are unstable with respect to spontaneous decomposition into a surface composed of two or more other orientations even though surface area may be increased. The latter depends on the surface tension of the crystal face in question, and little information on criteria of stability exists for the GaAs system. A kinetic theory of faceting implies a variation of evaporation rate with orientation or, alternately, a nucleation barrier arising from associated free energy from defects. The latter would result in only occasional facets on the epitaxy surface, while the former offered a more reasonable approach to understanding faceting on the (110) GaAs surface when grown by MBE. Thermodynamic and kinetic approaches to explain faceting in Cu and other metals are well established and can be found in numerous textbooks [21,22].

Compound semiconductor research on (110)GaAs involved careful examination of the influence of each MBE growth parameter on surface morphology and electronic/optical behavior. This systematic approach enabled the determination of the optimal growth conditions for further examination of the faceted epitaxy [18]. Optimal growth parameters were established through optical Nomarski microscopy, variable temperature Hall effect, and liquid He photoluminescence (PL). The nature of the observed faceting was then determined through LAUE x-ray diffraction, scanning electron microscopy (SEM), high resolution transmission electron microscopy and convergent beam electron diffraction (HREM, CBED), AUGER microanalysis and secondary ion mass spectroscopy in conjunction with standard crystallography [23,24]. The initial growth of the facets were also examined for (110) GaAs as well as on angled substrates, slightly off of (110), which exposed ledges of different chemical nature. A theory of facet initiation and formation was developed and a proven method for device quality growth of (110) GaAs/GaAs was established [25], verified through additional measurements of capacitance-voltage (CV) and deep level transient spectroscopy (DLTS) response. Finally, the results have led to the successful development of a GaAs/AlGaAs superlattice structure and a simple device fabricated in the (110) orientation with predictable doping profiles and electrical/optical behavior. The latter leads the way for further processing of (110) epitaxial device structures.

The following chapters outline the research involved with each phase of the (110) MBE epitaxy study. Morphology, optical and

electrical response, facet structure, kinetic processes of facet formation, elimination of the facets, and finally, device structures are discussed.

II. EXPERIMENTAL

Both 2° off-axis (100) and 2° off-axis (110) GaAs substrates grown by the Czockralski technique were obtained from Hewlett-Packard Optoelectronics Laboratory in Palo Alto, CA, for use in the following experiments. The (100) wafers would serve as a standard for each MBE growth run when grown on simultaneously with the (110) substrates. Epitaxy quality for devices grown on (100) substrates was well documented for a wide range of growth conditions, and optimal growth parameters for MBE (100) GaAs were established [26]. Substrates utilized were semi-insulating (110) and semi-insulating (100) GaAs. The first set of experiments described here which determine optimal growth parameters for (110) GaAs, however, used Cr-doped (100) GaAs standards. The surface defect count for the wafers was ~9 X $10^3/cm^2$.

Growth of GaAs epitaxy by MBE was performed in a Varian Gen II machine at the Varian III-V Device Center in Santa Clara, CA. The Gen II used had a base pressure of ~$1X10^{-10}$ Torr. A VANZETTI dual wavelength infrared pyrometer [27] was added outside the MBE growth chamber and hooked up with the HP1000 computer controls. The 2.04μm and 1.64μm pyrometer was tested with a blackbody radiation source for accurate temperature readings and verification of the MBE substrate thermocouple. Five molybdenum blocks were tested for substrate temperature (T_s) accuracy by watching for Si/Al alloying on an In bonded Si substrate with evaporated Al dots. The rotating molybdenum blocks would serve as GaAs substrate holders with In as a bonder.

Before transferring the (100) and (110) GaAs substrates into the MBE loading chamber, the wafers were etched in a solution of

$H_2SO_4:H_2O_2:H_2O$ ~ 8:1:1 for 3 minutes. This was followed by a DI water rinse for 3-5 minutes, a dip in a 1:10 solution of $NH_4OH:H_2O$ for 30 seconds, another DI water rinse for 3 minutes and then a spin dry. A surface oxide was subsequently formed in warm DI water for 1 min., again spin dried, and immediately loaded into the MBE chamber. The substrates were heated to 580°C in the MBE analytical chamber for 15 minutes to desorb any surface carbons, transferred to the growth chamber and heat cleaned at 630°C for 15 minutes to desorb any remaining oxygen and carbons. The As oven opened at T_s~550°C to prevent As desorption from the wafer surface. Si was used as the dopant for the epitaxial material, with an intended conductivity level of N_d ~ 5 X $10^{15}/cm^3$. The temperatures of the modified Knudson cells which contained the molecular beam constituents were: T_{As4} = 320°C, T_{Ga} = 1201°C, and T_{Si4} = 1100°C. This yielded a typical beam flux of P_{As4} = 1.1 X 10^{-5}Torr and P_{Ga} = 8.6 X 10^{-7} Torr. The Ga flux rate determines the growth rate of the epitaxy.

In order to determine the optimal growth conditions for the (110) GaAs, initial parameters of substrate growth temperature, arsenic overpressure, and growth rate were examined. T_s ranged from 510°C to 600°C, arsenic overpressure ranged from As/Ga atom ratios of 8/1 to 18/1, and growth rate varied from 1.4 microns/hr to 3.5 microns/hr.

Optical Nomarski microscopy, SEM, variable temperature Hall effect, and liquid He PL was utilized to examine the quality of the grown films to determine the optimal growth parameters. For the Hall effect, In dots were placed on ~1 cm^2 samples and alloyed at 420°C

for 20 minutes in a H_2 atmosphere to create the ohmic contacts. Hall measurements were carried out at 5KG. PL measurements were performed at sample temperatures of <4K using the excitation of a 676nm line from a krypton laser at 25 mW. The light beam was mechanically chopped and the sample luminescence was dispersed with a 1m SPEX monochrometer and detected with a dry ice cooled S-1 photomultiplier using standard lock-in methods. The S-1 photomultiplier is able to detect wavelengths from ~ 5,000 to 10,000 Å. With a 1200 line/mm spectrometer grating and 0.4mm slit, the system resolution was ~ 1.6 Å.

When examined by the above techniques, the substrate temperature which yielded the best electrical and optical responses would then be combined with a range of arsenic overpressures. The combination which yielded the best responses was then tested with the range of growth rates mentioned above. The combination of growth conditions which yielded the lowest surface defect count, the highest electron mobilities, and the best luminescence was considered to be the optimal growth parameters for (110) GaAs, even though the surface was still faceted.

For the next phase of the GaAs facet analysis, the (110) and (100) GaAs epitaxy was examined with respect to the facet geometry and their chemical composition. A JEOL SEM equipped with a tilting stage was utilized to tilt the (110) GaAs epitaxy in order to determine the angles of the facet sides with respect to the (110) surface. The formula devised for this purpose is outlined in Appendix I. Latex balls 0.2 microns in diameter were used to make certain that the

facets were growing from and not into the GaAs surface. A Phillips 400 TEM was used to view the faceted surfaces in plan-view and cross-section. Sample preparation methods for each process are outlined in Appendix II. Initial Laue X-ray diffraction results (in conjunction with SEM) of the facet crystal orientation were verified by the plan-view TEM. CBED on the Phillips 400 TEM was performed to determine the exact nature of the (111) back facet plane approximated from the tilting analysis. Cross-sections of faceted (110) GaAs were prepared such that the transmission electron beam was parallel to [1$\bar{1}$0]. In addition, cross-sections from GaAs wafers which were known to terminate with As and with Ga planes were also prepared to serve as references. Two methods were explored to determine the Ga or As character of the facet plane [28,29]: one utilized the (200) systematic row in the CBED pattern, and the other method depends on the image in the full <011> zone axis CBED pattern where the (200) and ($\bar{2}$00) disks contain different information because of the GaAs structure factor. The experiments marked the first time that such CBED information was used to determine the exact polarity of a <111> plane in GaAs [23]. HREM lattice images from a JEOL 200CX verified the correctly approximated facet planes of the SEM experiments. Crystallographic orientations were determined with respect to a standard FCC (110) stereographic projection which was used consistently throughout this investigation [30].

The faceted (110) GaAs epitaxy was also examined with a Phi AUGER system to determine the atomic percent of Ga and As in the epilayer. This was done in order to address the question of Ga clustering in the

epitaxy. SIMS was also performed on the (110) faceted epitaxy to verify these results and to examine the Si doping uniformity.

In order to better understand the kinetics and thermodynamics of the facet development, it was then necessary to examine the initial facet formation on the (110) GaAs substrates as compared to the (100) epitaxial growth. Separate MBE runs of 100 Å, 700 Å, and 1500 Å of GaAs epitaxy were grown on the (110) and (100) substrates. These layers were examined with the JEOL SEM to determine the growth progression of the facets. A kinetic understanding of initial facet formation was developed, based on the facet geometry with respect to the (110) GaAs crystal, the chemical nature of the facets, and the initial facet formation studies.

The model for facet initiation and development was further examined by analyzing the effect of the chemical nature of the (110) GaAs surface on the epitaxy morphology. Ledges on the GaAs substrate were introduced on the crystal by angling the substrate 6 degrees off-axis towards each of four different planes: (100), (010), (111), and $(11\bar{1})$. These four directions of substrate angling can be seen in the standard FCC (110) stereographic projection and provide very different chemical character to the (110) GaAs surface. Epitaxial films of 100 Å, 700 Å, and 1500 Å were grown on each substrate orientation as well as on the (100) GaAs substrate standard. Results of each growth were again examined with a JOEL SEM. Use of the novel CBED application allowed differentiation between the nature of the ledges on the substrate angled 6 degrees toward (111) and the substrate angled 6 degrees towards $(11\bar{1})$.

The successful off-axis substrate orientation which produced 1500 Å films of excellent morphology was then used to grow 1 micron films intentionally doped with Si (N_d ~ 5 X $10^{15}/cm^3$). Reliability of electrical and optical response were then tested by variable temperature Hall effect and liquid He PL. Capacitance-voltage characteristics verified the doping level and I-V measurements evaluated device response. The electron traps in these layers were characterized by capacitance DLTS using a double boxcar integrator [31]. For the CV, IV, and DLTS measurements on the (110) and (100) wafers, both evaporated AuGe ohmic contacts (0.15 microns) which were annealed at 450°C for 40 sec. and evaporated Au Schottky contacts were obtained by lithography techniques and are outlined in Appendix III. Films were examined by SEM and TEM.

Finally, the successful off-axis orientation and growth parameters were used to grow a superlattice of GaAs/AlGaAs. The superlattice layers alternated between 300 Å of AlgaAs and decreasing thicknesses of GaAs to a 10 Å GaAs cap. The superlattice was examined in cross-section on a Jeol 200CX TEM to determine the accuracy of each layer thickness . Room temperature photoluminescence verified Al mole fraction content. (110) GaAs MESFETS were also fabricated. The MESFET processing utilized e- beam direct writing to define the gate and conventional masking to create the AuGe ohmic contacts and further isolation. CV measurements were performed to determine doping levels in the n^+ cap and n-channel regions.

III. OPTIMAL GROWTH CONDITIONS FOR (110) GaAs AS COMPARED TO (100) GaAs

In order to determine the optimal MBE growth parameters for the (110) GaAs epitaxy, material performance was compared to a standard (100) GaAs epitaxy grown simultaneously with the (110) GaAs. The primary MBE growth variables that were easily controlled by the operator were explored and their influence on material behavior was researched.

The substrate temperature, T_s, was changed from 590°C to 570°C to 550°C to 510°C in four growth runs. The optical Nomarski photographs for each of the (110) GaAs epitaxy surfaces are shown in Figure 1. Epitaxy faceting occurred in all cases of T_s variation. A defect count revealed that, instead of decreasing the initial substrate dislocation density of $\sim 9 \times 10^3/cm^2$, the epitaxy of all T_s growth runs increased the defect count to over 10^4-$10^5/cm^2$ for each of them. In order of decreasing T_s, defect counts were $9.9 \times 10^4/cm^2$, $9.1 \times 10^4/cm^2$, $1.8 \times 10^5/cm^2$, and $3.6 \times 10^5/cm^2$. The substrate growth temperature of 570°C yielded the best surface morphology. The As/Ga ratio was ~8/1 and a standard growth rate of 1.4 microns/hr was used.

Figure 2 shows the Nomarski optical photographs of the surface morphology for the GaAs epitaxy grown with increased arsenic overpressure. The substrate temperatures were 570°C and 550°C, respectively. The arsenic overpressure was increased by 50%. Any further increase in arsenic overpressure would coat the viewports and associated instrumentation of the growth chamber. Once again, epitaxy defect

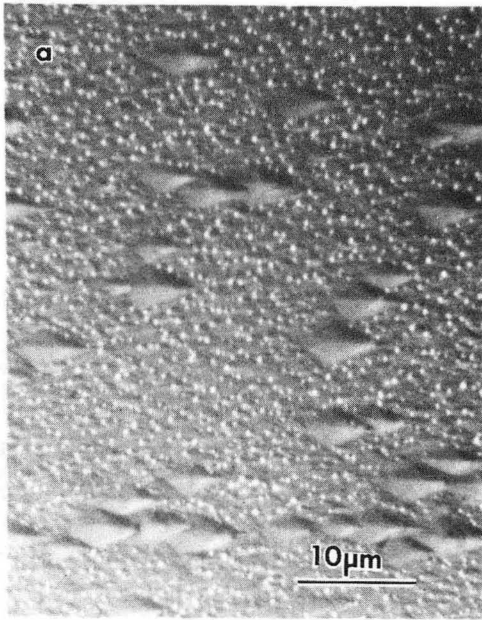

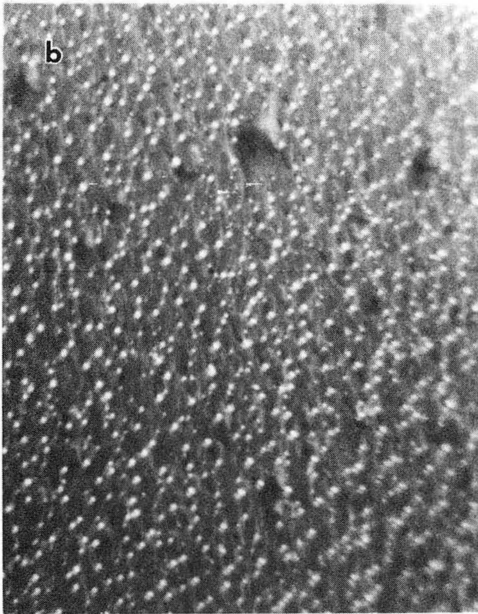

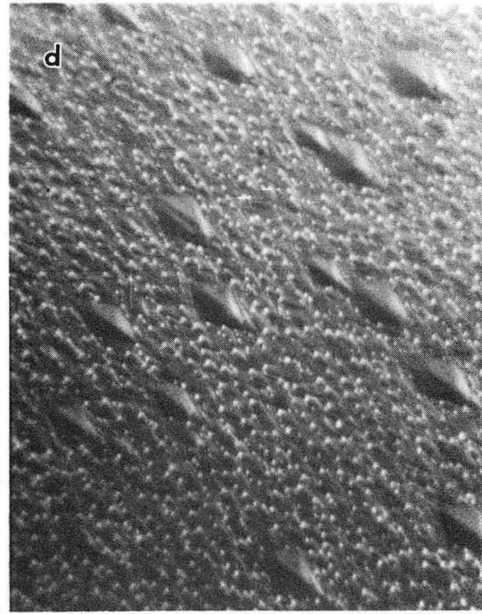

XBB 860-9608

Figure 1

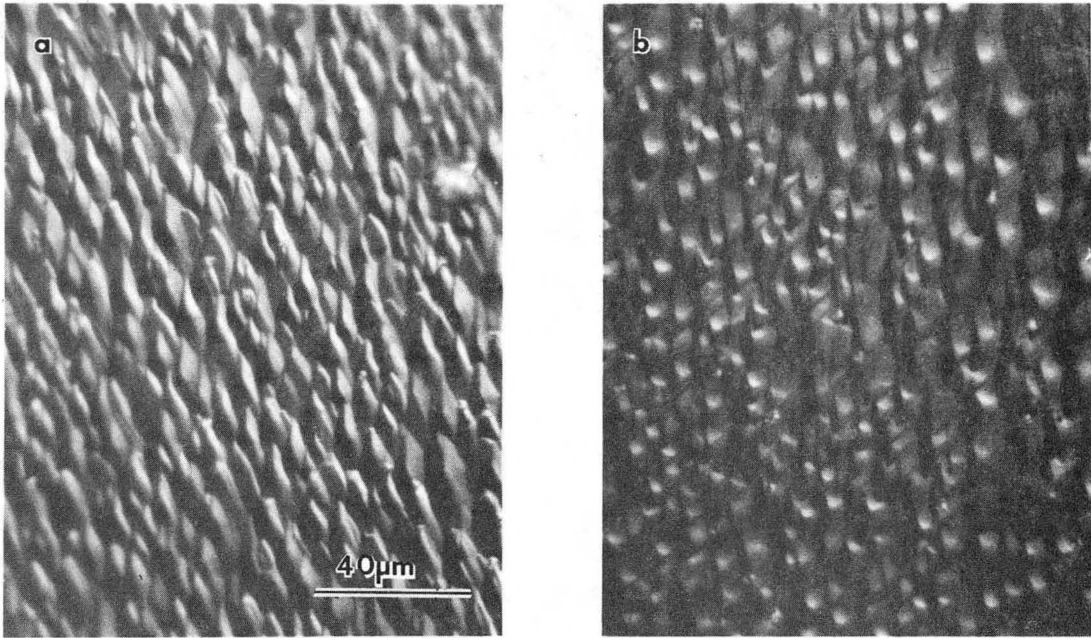

XBB 860-9604

Figure 2

density of ~ $10^5/cm^2$ was increased over substrate defect density, but smaller facets had resulted from the change in this growth parameter with T_s=570°C.

Figure 3 shows the surface morphology of the (110) epitaxial layers with a variation of growth rate and otherwise optimal growth parameters of T_s=570°C and As/Ga=8/1. Variation of growth rate seemed to have no effect on the surface quality. As in all cases of changing growth parameters, the (100) standard GaAs epitaxy appeared smooth and shiny.

Figure 4 shows the Nomarski optical photograph of the (110) GaAs epitaxy grown under the combined parameters of T_s = 570°C, As/Ga = 12/1, and growth rate = .35 microns/hr. The surface morphology is still of poor quality, and surface defect counts were not satisfactory.

The Hall effect data for all cases of the (110) GaAs epitaxy and the (100) epitaxy are shown in Table I. The simultaneously grown (100) layers indicated incorporation of the intentional doping concentration of ~ $5X10^{15}/cm^3$ for each of the substrate growth temperatures. Mobility of the electrons decreased and free carrier concentrations slightly increased with decreasing substrate temperature. Free carrier concentrations were confirmed with capacitance-voltage measurements. For the (110) epitaxy, the free carrier concentration exhibited anomalously high conductivity at room temperature for all substrate growth temperatures. While the planned doping concentrations were in the mid $10^{15}/cm^3$ range, the (110) GaAs epitaxy consistently showed free carrier concentrations of low $10^{17}/cm^3$. Carrier freezeout

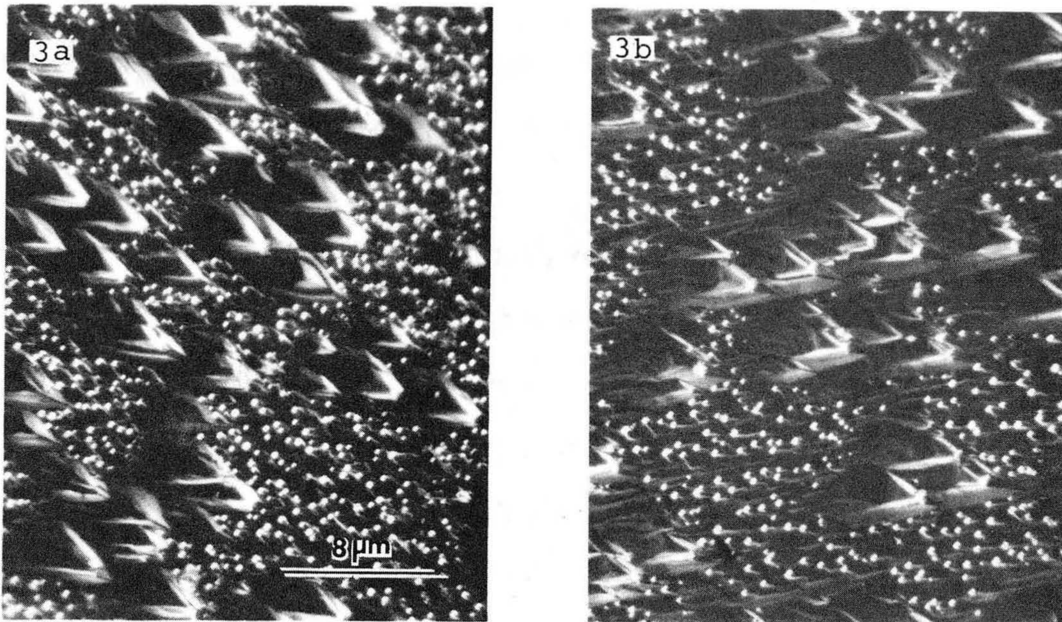

Figure 3

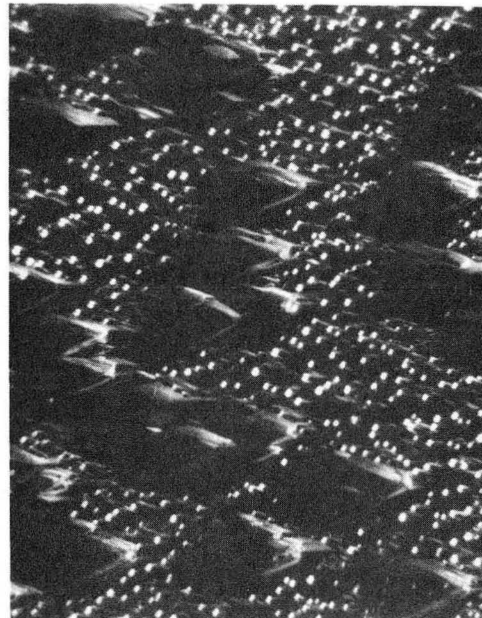

XBB 860-9609

Figure 4

TABLE 1. HALL EFFECT DATA and PL PEAK RATIOS

Substr. Temp (C)	Substr. Orient.	Room Temp carrier conc. (cm-3)	Room Temp Mobility (cm2/V-s)	Liquid N2 carrier conc. (cm-3)	Liquid N2 Mobility (cm2/V-s)
590	(100)	n=7.97E15	5926	N=9.30E15	21511
570	(100)	n=8,59E15	5615	N=9.40E15	20412
550	(100)	n=8.88E15	5472	N=9.50E15	20135
510	(100)	n=9.47E15	4643	N=1.00E10	3465
590	(110)	n=2.10E17	1446	FREEZEOUT	---
570	(110)	N=1.50E17	1779	FREEZEOUT	---
550	(100)	N=1.00E17	368	FREEZEOUT	---
510	(110)	P=8.20E15	172	P=1.40E10	6044
vairable: increased As flux					
570	(100)	N=1.04E16	5218	N=1.13E15	18462
550	(100)	N=1.05E16	4979	N=1.13E16	17354
570	(110)	N=2.30E17	2018	N=9.10E15	4480
550	(110)	N=2.90E18	2219	FREEZEOUT	---
variable: growth rate					
570,1/2	(100)	N=6.90E15	4585	N=8.20E15	17772
570,1/4	(100)	N=7.50E15	5097	N=8.70E15	18252
570,1/2	(110)	N=1.49E20	1709	N=2.10E20	388
570,1/4	(110)	N=3.10E18	1997	N=1.50E18	170
variables: 1/4 growth rate, increased As flux					
570	(100)	N=8.00E15	5041	N=9.60E15	18673
570	(110)	N=1.00E17	1038	N=2.50E14	2462

was experienced at liquid nitrogen temperatures. The amphoteric doping behavior of Si became apparent at 510°C where the material was p-type with a nearly insulating free carrier concentration of $10^{10}/cm^3$ and extremely poor mobilities. It is not surprising that the Si preferred the As site with these growth conditions which were Ga-rich [17], especially with decreased physisorption times. An increase in the As flux aided in the probability of Ga site chemisorption of the Si without an accompanying freezeout of free carrier concentration at 77K from a highly compensating acceptor level. This was true for the growth with an increased As overpressure. With this increased As overpressure, the (100) GaAs epitaxy decreased in electrical performance. The (110) GaAs epitaxy, however, showed some improvement in electron mobility and carrier type but still exhibited unpredictable doping levels. A reduction in growth rate did not improve the (100) GaAs standard free carrier concentration or increase the mobilities. The same held true for the (110) GaAs epitaxy, but it was noted that the slower growth rate did inhibit carrier freezeout at 77K. The mobility was sharply decreased at the lower temperature. The combination of growth parameters held no advantage for either carrier concentration or room temperature mobility.

A temperature dependent Hall effect plot of free carrier concentration vs. temperature for the (110) epitaxy grown under optimal growth conditions is shown in Figure 5. The results are compared to the (100) GaAs standard material simultaneously grown. The characteristic carrier freezeout in the (110) GaAs film has an activation

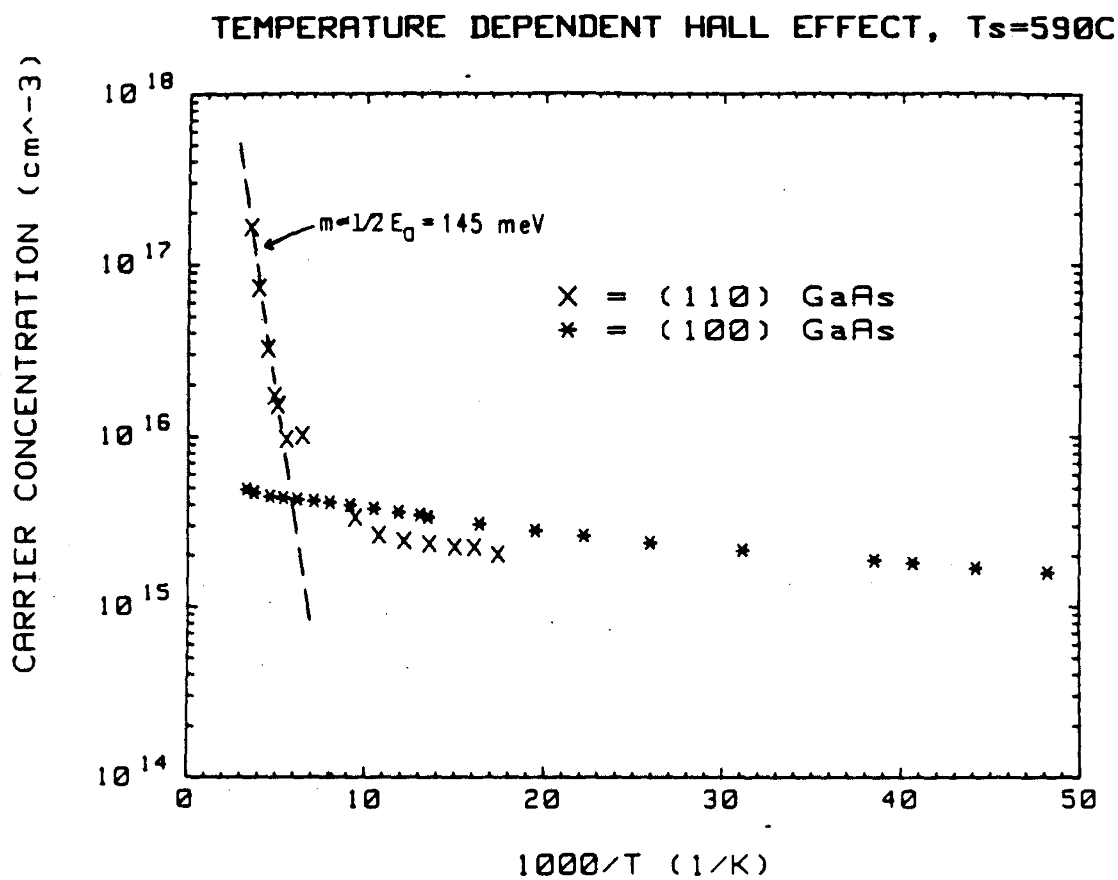

Figure 5

energy of ~ 145 meV corresponding to a deep donor level at ~ 290 meV. This Hall effect data indicated that, at room temperature, electrical conduction in the (110) film is due to the presence of the deeper donor. At lower temperatures, a partially compensating acceptor level of ~ $2x10^{15}/cm^3$ was discovered by the extrinsic slope of the Hall plot. This could be confirmed with a DLTS measurement. The acceptor level in discussion was of the same order of magnitude as that of the intentionally doped Si for those samples which froze out at 77K. Thus, at or below liquid N2 temperatures, the deeper donor level and the Si n-type level were, respectively, frozen out and compensated.

This apparent compensation level which was present for each (110) GaAs epitaxy examined for various growth conditions is supported by the theory of Walukiewicz et al. [32]. They have studied the effect of compensation on the electron mobility in GaAs and provide computations of mobility which include all major scattering processes and screening effects. Their calculations provide a basis for determining the compensation ratio, or the total density of ionized impurities in n-type GaAs from independent room temperature measurements of the electron mobility and carrier concentration. Analyzing the Hall data in order to determine the compensating level present for the best case of (110) GaAs grown at 570°C with an increased As overpressure, the data shows that:

$$\mu_{HALL} = 1,289\ cm^2/V\text{-}sec$$

and

$$N_D = 2.46 \times 10^{17}/cm^3,$$

where μ_{HALL} is the Hall mobility of the free carriers and N_D is the free carrier n-type concentration. Utilizing the tables of [32], these measurements indicate a high compensation ratio, θ, of 0.78 in the epitaxy. The true ionization concentration, n_{ion}, can be found from their derived formula of:

$$n_{ion} = N_D (1+\theta)/(1-\theta) \tag{1}$$

where:

$$n_{ion} = \text{(total ionized impurity concentration)} - \text{(measured ionized impurity concentration)}. \tag{2}$$

Thus, for $\theta = 0.78$, the true ionized donor concentration in the (110) GaAs epitaxy is ($1.99 \times 10^{18}/cm^3$)! Therefore, the poor electron mobility of the (110) film must be governed, even at room temperature, by scattering centers which are ~ ($2.23 \times 10^{18}/cm^3$). While they may be ionized, they are obviously not conducting and so indicate that the compensation level in the n-type material is on the order of $10^{18}/cm^3$. The measured ionized impurity concentration of ($2.46 \times 10^{17}/cm^3$) are the conducting electrons and are most likely coming from the deep donor level found in all the (110) epitaxy.

The Hall effect data are compared to the liquid He PL studies whose curves are shown in Figure 6. Figure 6a shows the recombination emissions for the (110) and (100) substrate temperature variation, Figure 6b for that of increased As flux, Figure 6c for that of decreased growth rate, and Figure 6d shows those peaks obtained for the combination of growth parameters. For (100) GaAs epitaxy, the dominant peaks

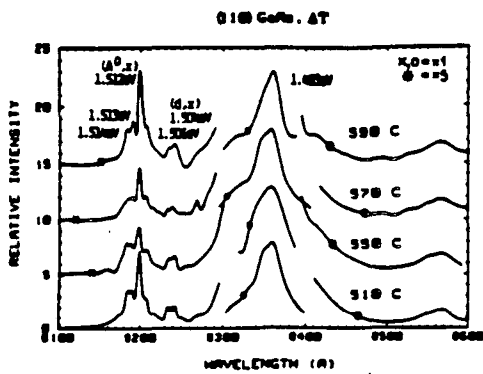

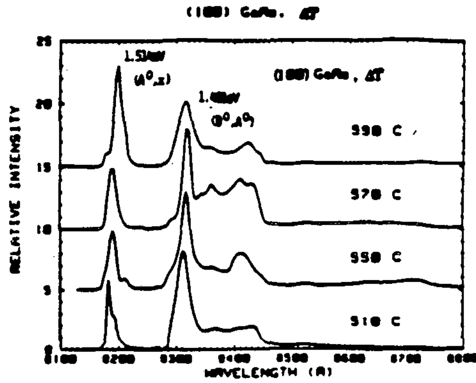

FIGURE : Liquid He PL intensities for variation in MBE substrate growth temperatures

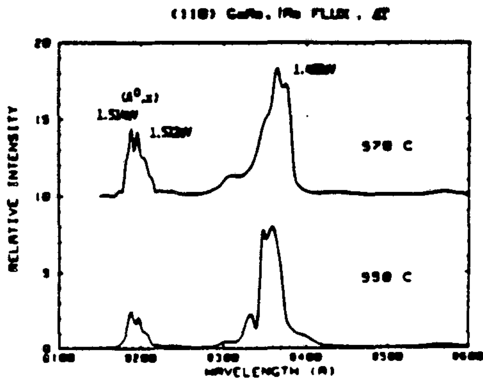

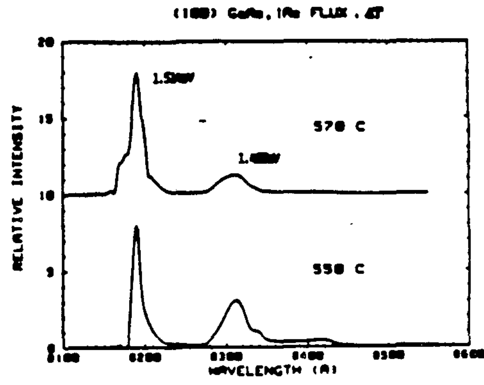

FIGURE : PL intensities for MBE epi layers with increased As_4 flux

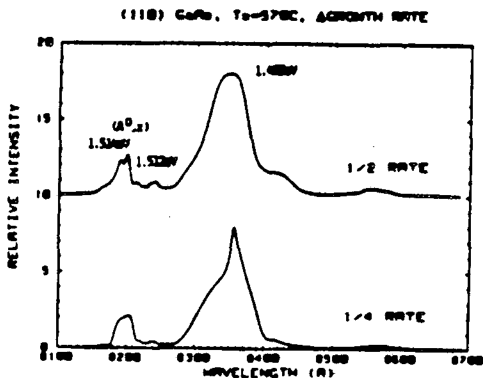

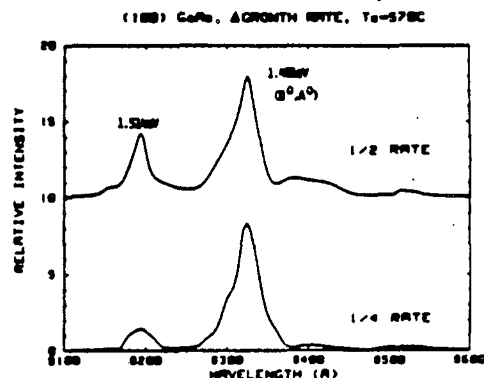

FIGURE : PL intensities for decreasing Ga flux (growth rate).

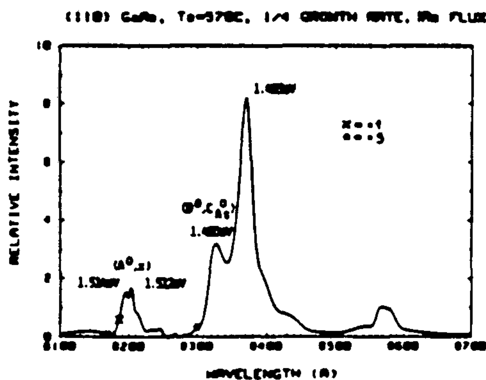

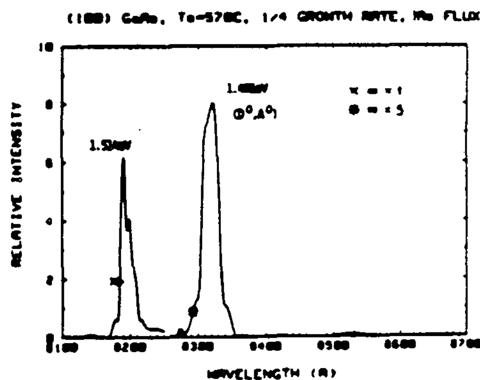

FIGURE : PL intensities for (110) and (100) GaAs epi layers grown with combination of optimized growth parameters.

Figure 6

appear at 1.514 eV and 1.491 eV. The 1.491 eV peak is associated with a neutral donor, neutral carbon acceptor (D°,C°_{As}) transition. The 1.5145 eV peak has been observed in other GaAs MBE material [33], and falls within the range of exciton, neutral acceptor (A°,x) transitions. In (110) GaAs, it is interesting to note the split peaks at 1.512-1.514 eV for all growth conditions. Again, these are associated with the exciton, neutral acceptor (A°,x) transitions. The 1.504 and 1.506 split peaks seen in the substrate temperature variations is thought to be the 'defect-induced' bound exciton (d,x) transition band as reported by Kunzel and Ploog [34]. The dominant peak at 1.483 eV is near to the conduction band, neutral Si acceptor (e,Si_{As}°) transition which supports the strong acceptor compensation speculated in the Hall effect data. The small 1.448 eV peak is thought to be the Si LO phonon replica reported by Wang [16] and others.

A strong exciton peak for both (100) and (110) GaAs epitaxy is indicative of high quality epitaxial material. The dominance of the exciton, neutral acceptor (A°,x) luminescence for either material suggests that bound excitons are present in the epitaxy and have not been influenced by the presence of strain fields or non-radiative recombination centers. Such defects will greatly reduce the number of bound excitons in the material by giving the bound electron enough energy to become free or to recombine. A relative intensity comparison between the dominant neutral acceptor (e,Si_{As}°) transition at 1.483 eV and the exciton, neutral acceptor (x,A°) transition at 1.514 eV for the (110) material was a measure of that material quality.

Similarly, for the (100) GaAs standard, the relative peak heights of the 1.491 eV (D°,A°) transition to the 1.514 eV (A°,x) transition was compared.

For the (100) GaAs standard film, the material degrades slightly with a decrease in substrate temperature, with a decrease in substrate temperature combined with higher arsenic overpressure, with a decrease in growth rate, and with the combination of the above growth parameters. This was evidenced by the decrease in the exciton peak intensities and dominance of the neutral donor, neutral acceptor transitions. The Hall data reflected the degradation in material quality with the decrease in carrier mobility. For the (110) GaAs epitaxy, a great improvement in peak ratio was seen for growth with and increased As overpressure for the substrate temperature of 570°C. For the same growth conditions, the 'defect-induced' bound exciton transitions disappear, as well. This correlates well with the Hall effect data in that the highest mobility was found for the same growth conditions. The combination of growth parameters did not improve the GaAs epitaxy over the growth at 570°C with increased As overpressure for the (110) material. In fact, the material showed the lowest exciton luminescence with respect to the neutral donor, neutral acceptor transition and did not exhibit the high electron mobility of the normal growth rate.

The results of the various growth conditions for the (110) GaAs epitaxy show a good correlation between the morphology as observed by optical Nomarski microscopy, the electrical behavior as shown through Hall effect measurements, and the optical response as exhibited by the

luminescence of the films. From the above studies, all further films were grown at 570–580°C with an increased arsenic overpressure yielding As/Ga = 12–16/1. Because the growth rate did not influence material performance, the standard growth rate was used for all later runs.

IV. THE NATURE OF (110) GaAs FACETING

The (110) GaAs epitaxy was then examined in order to better understand the nature of the faceting phenomenon. Facet crystal geometry was determined with respect to the (110) GaAs surface and the chemical nature of the facets were found. This information was important in determining the probable causes of faceting during growth on the (110) GaAs surface.

The facets were examined by SEM in conjunction with Laue x-ray diffraction to determine their general orientation with respect to the FCC (110) stereographic projection reference. As indicated in the SEM image at 6000X in Figure 7, the facets were found to lie along [001] and this was true for all (110) faceting cases. Facets were found to be from <1 micron to >10 microns in length, and from 0.5 to 8 microns wide. Several large facets had peculiar tips which were examined more closely with other microscopy techniques. Figure 8 shows an SEM image of a facet which has been brushed with dried, spherical polymer particles from acrylic latex with ~ .2 micron diameter. The latex particle chain shows the distinctive hillock vs.pitted nature of the facets.

Plan-view TEM samples verified the facet orientation, as shown in the complete two-beam image series of Figure 9. Figure 9a-9d shows the two-beam or systematic row images with the corresponding diffraction pattern in the 200, 220, 111-right, and 111-left orientations of the crystal. Seen is a thinned facet in the (110) GaAs epitaxy with numerous dislocations in the surrounding material. The thickness fringes of the images suggested that the tip of the facet, in dark

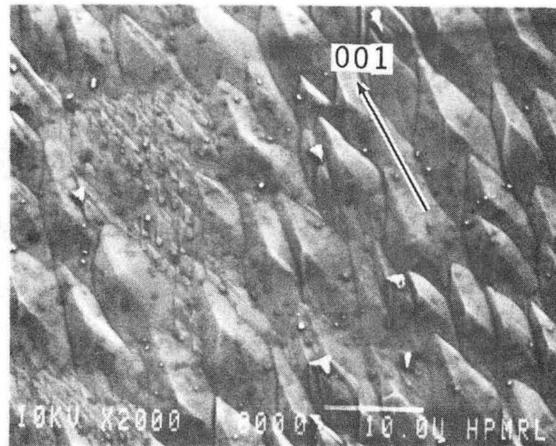

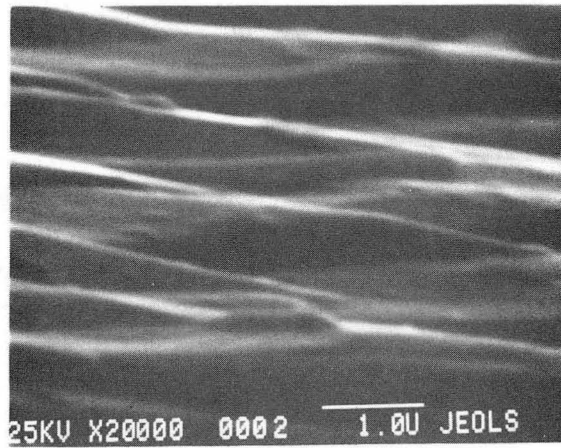

XBB 860-9598

Figure 7

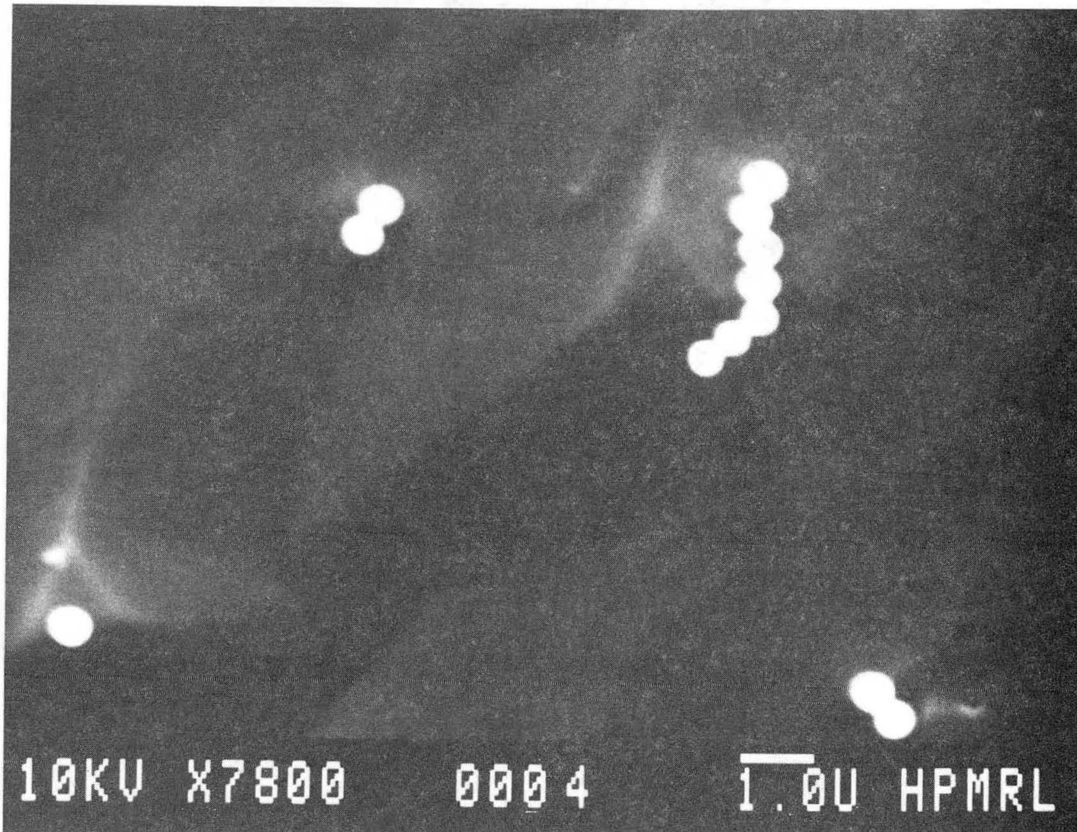

XBB 860-9605

Figure 8

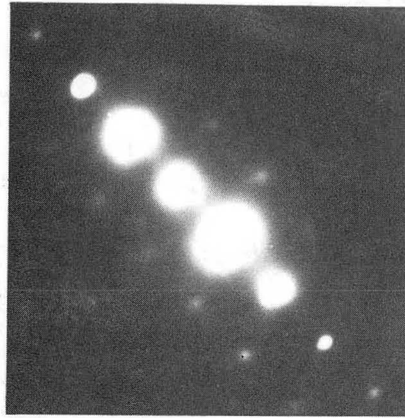

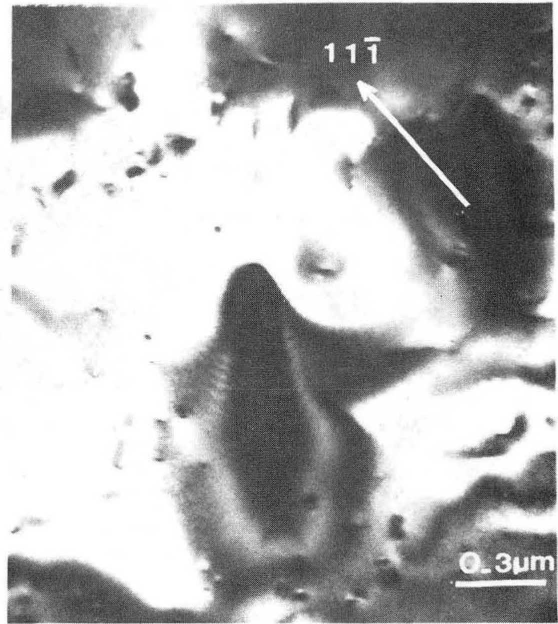

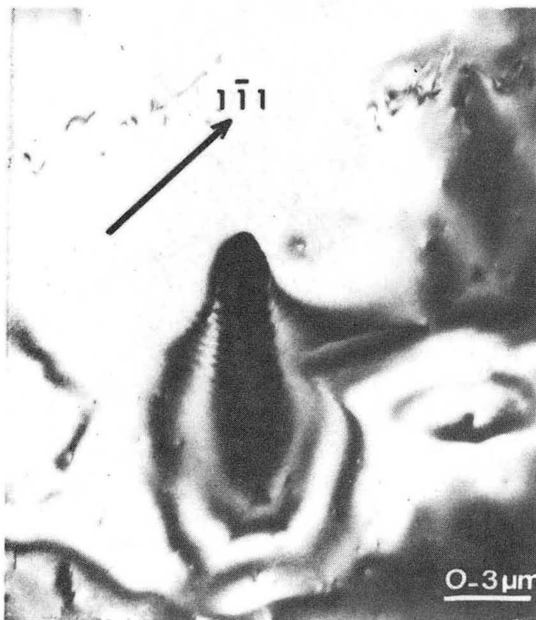

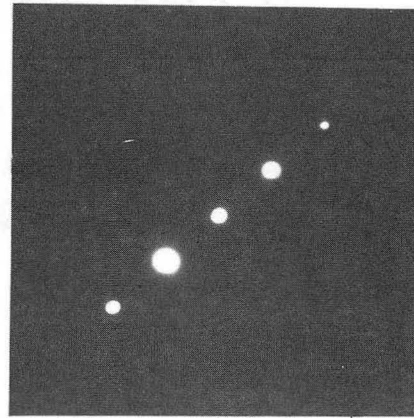

XBB 860-9603

Figure 9a,b

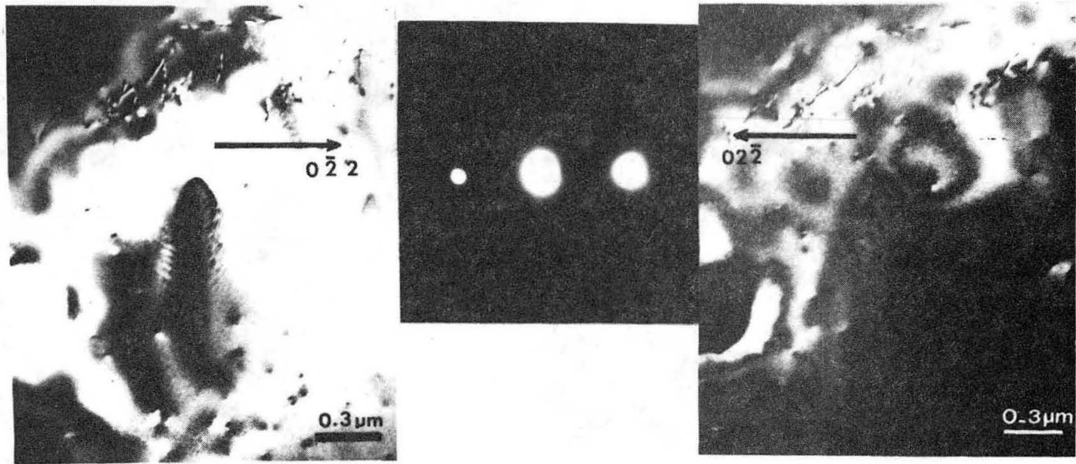

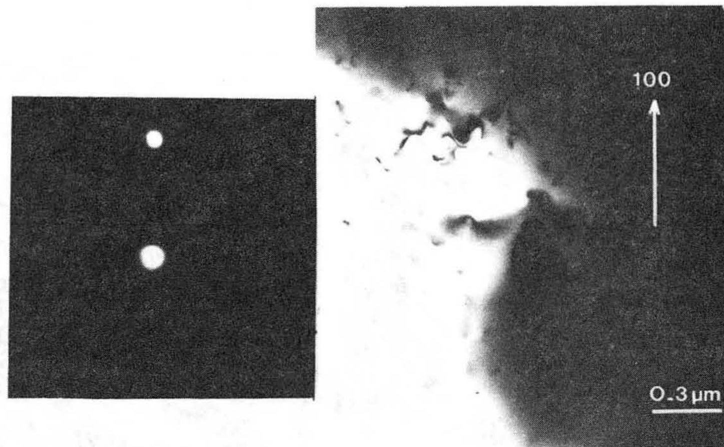

XBB 860-9602

Figure 9c,d

contrast, is the thicker end of the polyganal shape that thinned down near to the GaAs (110) surface in the back facet plane. Alternately, the dislocations in the material may have prevented this end of the facet to ion mill at the same rate as the rest of the object. The facets were not found to be misoriented with the GaAs epitaxy matrix as evidenced by microdiffraction techniques with a probesize of 200 Å. Thus, the dislocations shown in the 2-beam conditions, were calculated to be primarily Schokley partials of Burger's vector 1/6<112>, and were thought to result from the strain associated with the facet initiation as well as from dislocation propagation from the substrate.

Microdiffraction of the facet side, tip, middle, and surrounding, all show the 110 crystal orientation. Streaking in the microdiffraction pattern along the <111> direction was prevalent when the tip regions were examined. The twinning planes intersect the sample at an angle such that the Ewald sphere of the electron beam picked up partial streaking from the fault planes which are visible in the microdiffraction pattern. The streaks which are perpendicular to the habit plane of the corresponding fault are associated with the visible twinning in the facet tip. The streaking direction and visible twinning correlation is supported by Fourier analysis of diffraction patterns [35]. A full microdiffraction pattern and corresponding micrograph shown in Figure 10 exhibited isolated twin regions along the 111 axis at the facet tip outer periphery. The extra spots seen in the (110) microdiffraction pattern are also a result of the {111} twinning, with the mirror plane along the [111]-right. The facet tip is too

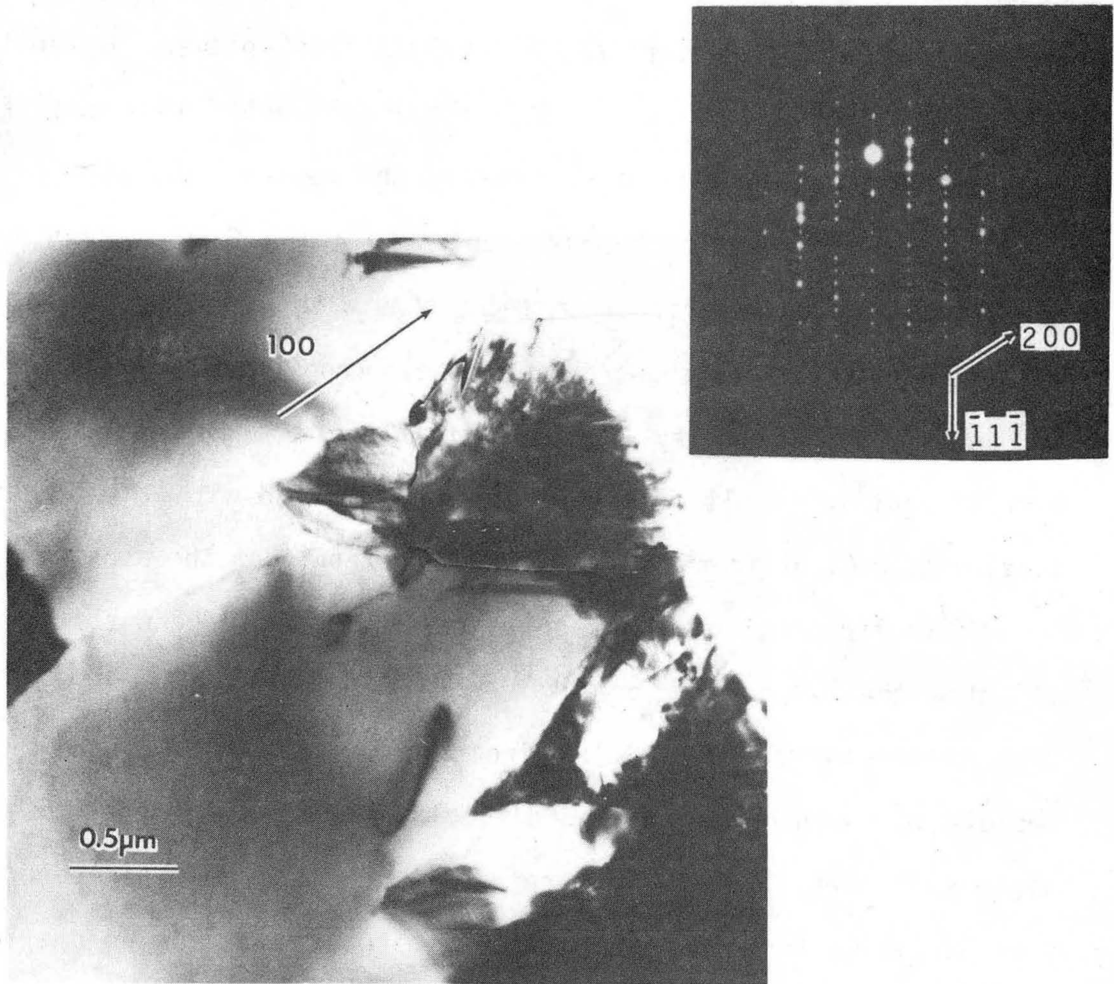

XBB 873-1986

Figure 10

thick for additional contrast information. Cross-sectional TEM images show the facets themselves to be replete with dislocations.

The SEM was utilized to determine the angles between the (110) GaAs substrate and the facet sides in order to calculate the Miller indices of the facet side planes. Placing the faceted samples as is described in Appendix I, tilting was performed as is shown in Figure 11 for 0°, 25° and 50° views of the surface. The tip of the facet referred to is the pointed, thicker end. From the measurements, both side planes appeared to be angled 45° from the (110) surface and the back planes of the facets averaged ~ 31° from the (110) epitaxy surface. This suggested that the side planes were of $\{100\}$ types and the back plane very close to the $\{111\}$ type plane at an angle of 35° from the surface. The low index facet sides and back are consistent with thermodynamically based faceting behavior in FCC metals [20] where a low surface tension is preferred. These facet sides and facet orientation were verified by HREM. A facet tip in high resolution is shown in Figure 12, showing that the very tip of the facet intersects the (110) GaAs along $\{111\}$ planes. The orientation is unmistakably along [001] and the side planes are verified, as well.

The determination of the crystal polarity of the facet surfaces was also important in order to better understand the facet formation process. For the facets, a particular application of the convergent beam electron diffraction method to identify the As and Ga planes in $\{110\}$ GaAs was used. It had already been shown that the specific features in convergent beam diffraction discs are rich in information

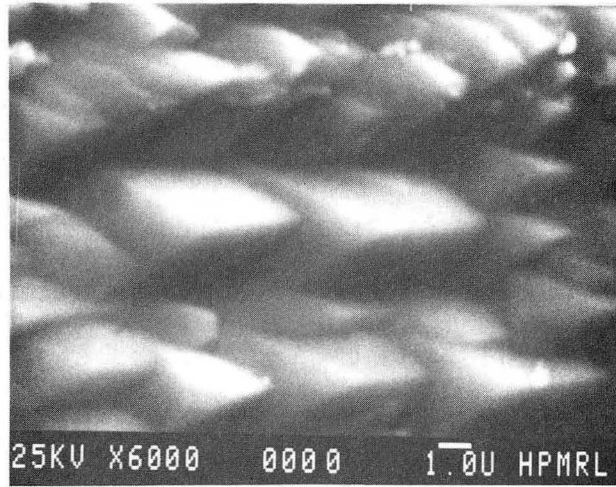

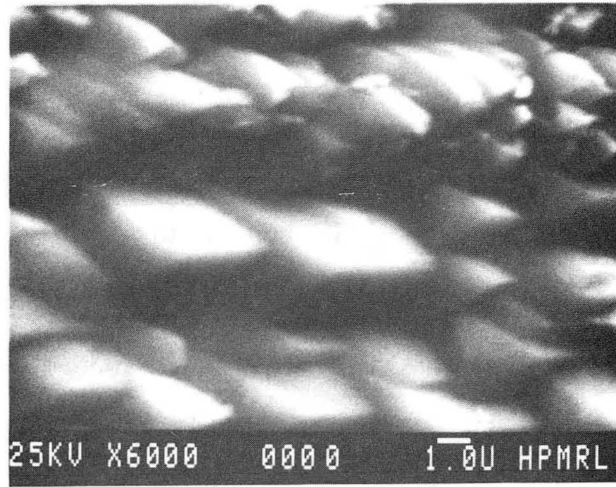

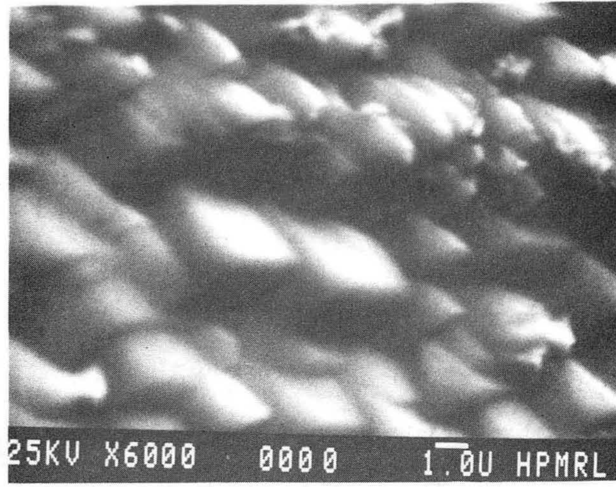

XBB 860-9599

Figure 11a

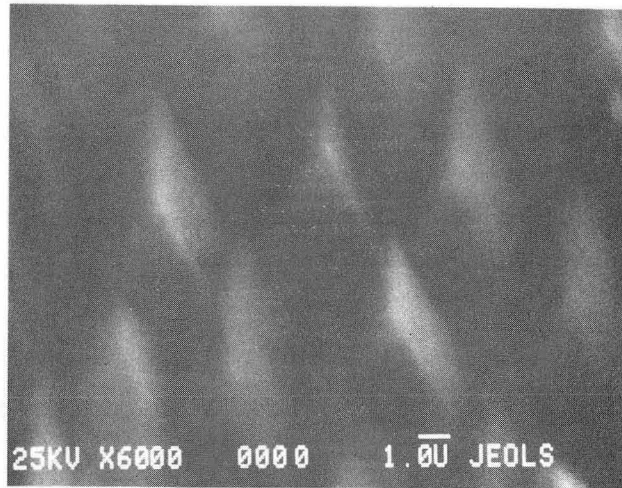

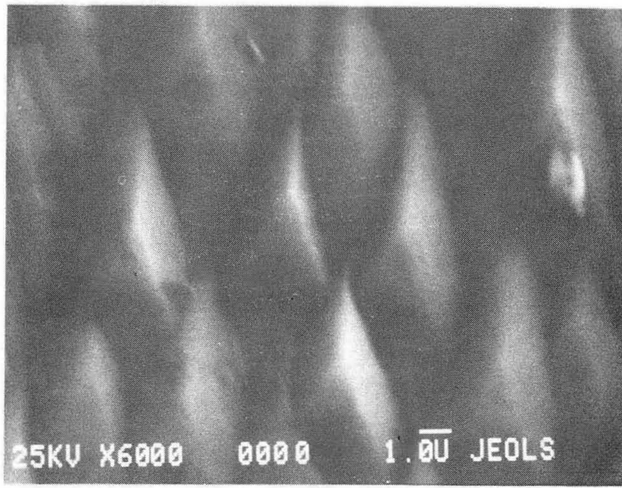

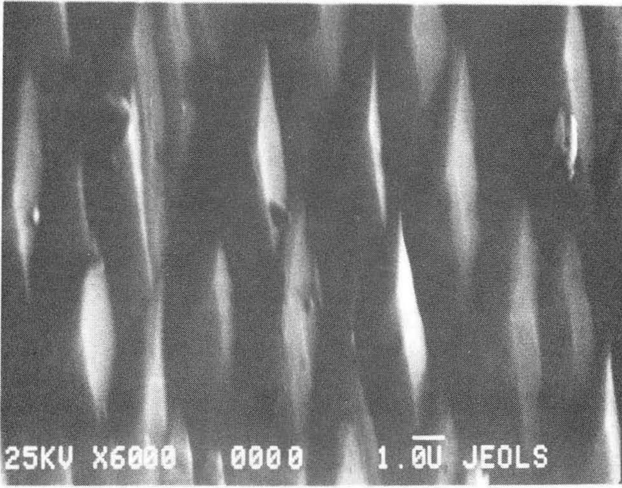

XBB 860-9607

Figure 11b

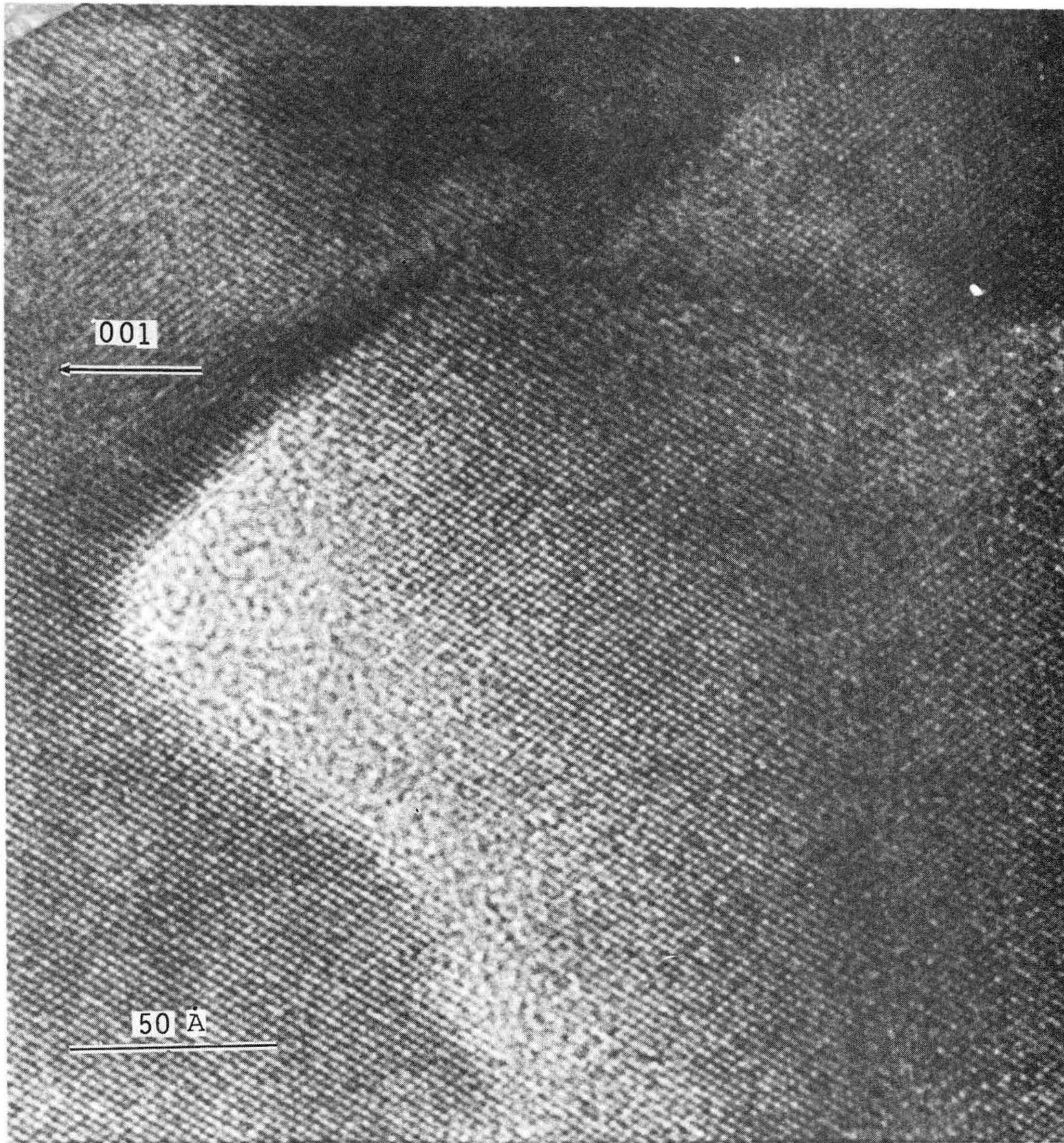

XBB 860-10403

Figure 12

about crystal structure [36], point groups [29], structure factors [37], and polarity of the crystal [28]. Information based on the structure factor of GaAs was found in the +200 and -200 beams of the convergent diffraction discs through white or black crosses observed there, as well as in the CBED pattern of the full (011) pole. Both methods were employed to determine the As or Ga nature of the back {111} surface of the facets. In this case, both {111}As and {111}Ga reference surfaces were prepared in cross-section to examine the full CBED pattern and the black or white crosses in the specific +200 and -200 CBED discs. For the method utilizing the (200) systematic row of the CBED pattern [28], the systematic (200) reflection was excited with two other reflections on the Ewald sphere that fulfilled the Bragg condition. Constructive or destructive interaction of the ($\bar{7}5\bar{5}$) and ($95\bar{5}$) beams resulted in the appearance of the white cross or black cross in the +200 or -200 convergent beam disc.

Figure 13a shows the {111}Ga and {111}As faces after a verification etch. Cross sections were prepared from the same substrates (unetched) and Figure 13b shows the results of the novel application of the distinguishing patterns in CBED of GaAs for the Ga and As surface references [23]. The pattern arrangement in the (200) disk of the systematic (200) CBED pattern or in the (011) zone axis CBED pattern depends on the specific positions of the As and Ga planes in the sample. In Figure 14, sample I shows the white cross, which correlated with the As plane, appeared in the (200) systematic disc. In the ($\bar{2}00$) disc, the black cross appeared correlated with the As plane.

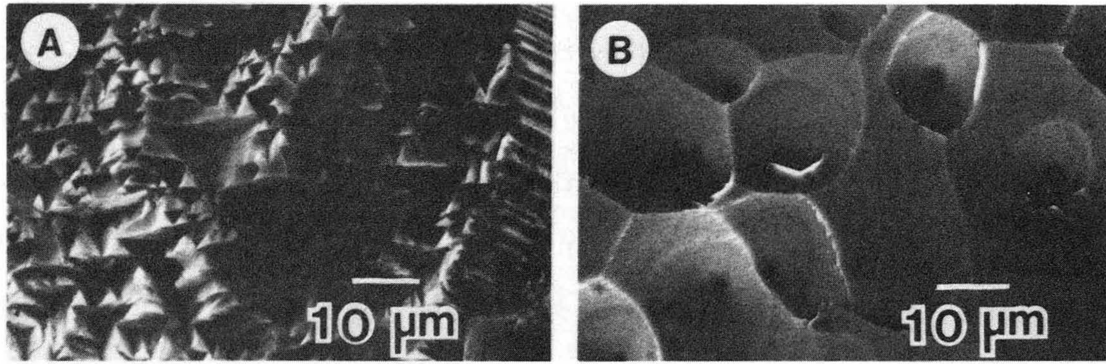

XBB 867-5485

Figure 13a

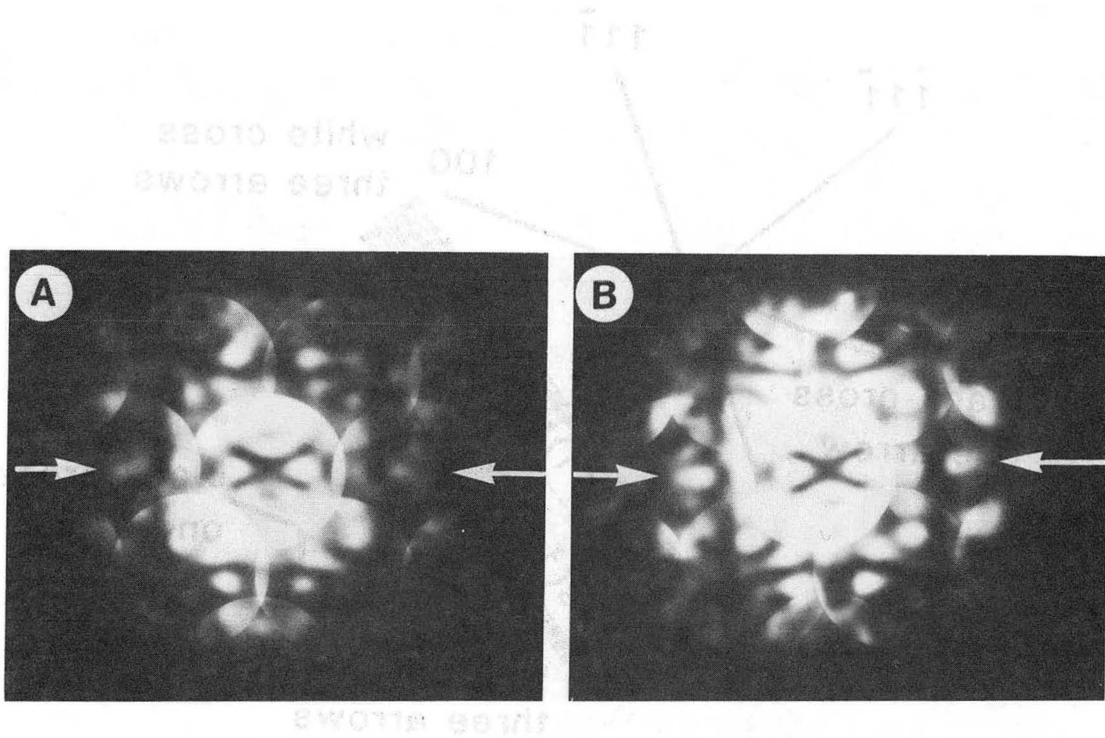

XBB 867-5485

Figure 13b

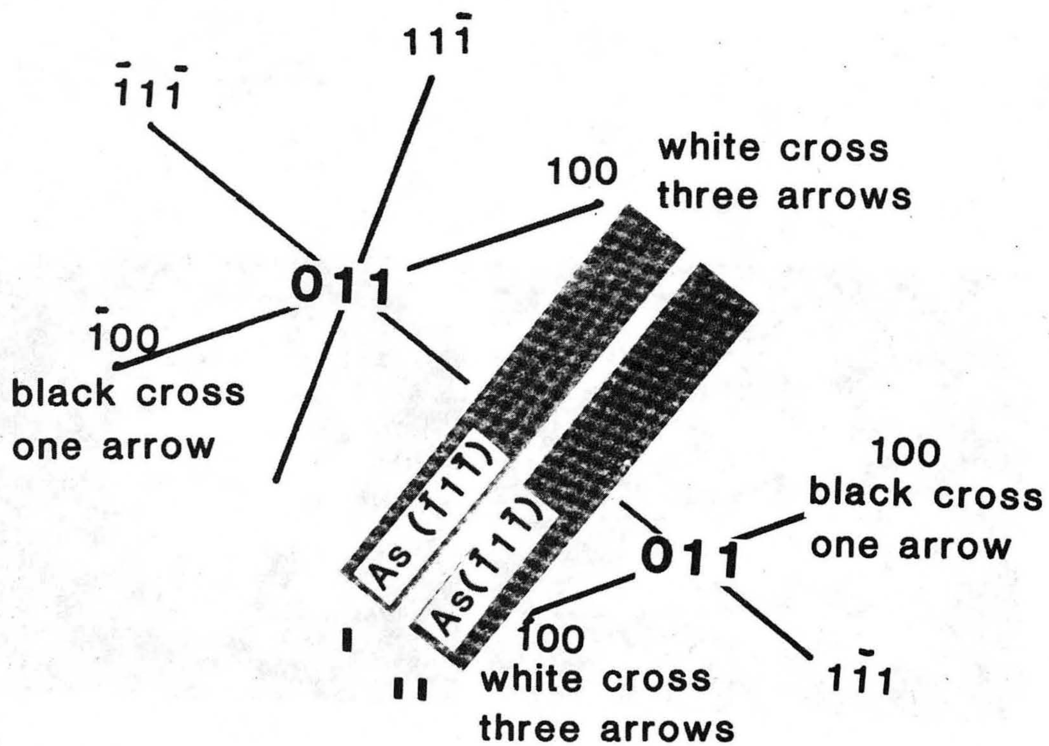

XBB 867-5384

Figure 14

The same is true for sample II: the white cross was always correlated with the arsenic plane. The (011) zone axis CBED pattern showed three arrows in the (200) disc which correlated with the As plane and one arrow in the ($\bar{2}$00) disc which correlated with the Ga plane. When the Ga $\{111\}$ planes were glued together, the results confirmed the changing contrast pattern. Different information existed in the 200 discs due to the location of the Ga planes vs. As planes. It was important to note that at no thickness of the GaAs samples did the observed patterns reverse contrast or change correlation. Sample thickness only made it difficult to observe the patterns if the specimen was too thick or thin. The information was referenced to the standard stereographic projection which is shown in Appendix IV.

Figure 15 shows the results of the above application to the faceted (110) GaAs sample. The sample was brought into the same CBED condition which was referenced above after taking an untilted bright field micrograph and diffraction pattern. The diffraction pattern of the facets were of the same camera length as the Ga and As standards, and were taken with the bright field images in the same TEM session. The facet images and diffraction patterns were matched up with the CBED information with respect to the starting point of the reference stereographic projection that the untilted (and unwarped sample area) diffraction pattern of the specimen indicated. From the same stereographic projection reference which was utilized for the standard reference calculations, the back plane of the facet was found to be always Ga-rich in nature. A final picture of the facet geometry and

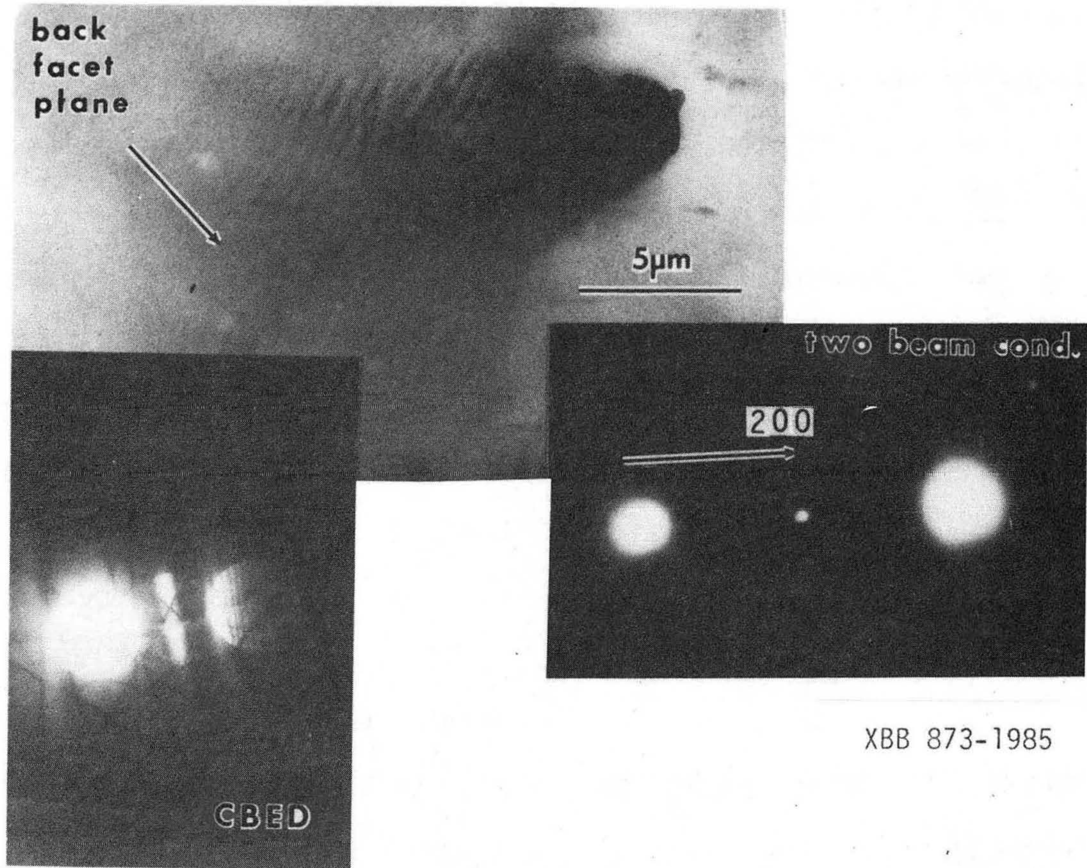

XBB 873-1985

Figure 15

crystal orientation with respect to the (110) stereographic projection for the GaAs FCC system is shown in Figure 16.

The chemical composition of the facets were examined by AUGER microscopy, SIMS, and microdiffraction EDAX techniques. Figure 17 shows a typical AUGER analysis of the facet composition as compared with the substrate (110) GaAs. Point No. 2 of the inset is shown and represents analysis of the middle of the facet with an As content sampled. The Ga content was internally calculated as the remainder of a 100% GaAs atomic content and explains the mirror symmetry of the Ga and As readings for each set. Points 1 and 3, the tip and back of the facet, were also examined but did not show any difference of atomic percent composition. The high resolution AUGER had a probe size of 2000Å and a sputter rate of 200Å/min. The analysis was performed with a 20KV accelerating voltage. SIMS of the faceted surface used oxygen ions with a 300Å beam size as the sputter source and traced the profiles of As, Si^{27} and Si^{28}. The profiles showed slight variations in Si content as a function of epitaxy depth with an average doping level of $1x10^{18}$ cm^{-3}, but the information concerning the film stoichiometry agreed with the AUGER analysis. SIMS utilized an analyzer voltage of 19KV with a sputter rate of 3Å/sec. A Sloan DEKTAK II measured the depth of the SIMS sputtered area. As Si diffusion was not appreciable at the growth temperature of the GaAs epitaxy [38], possible surface segregation of that element could not explain the results of the chemical analysis. Microdiffraction of various samples ruled out pipe diffusion as a source for isolated cases of Si accumulation, as not all facets with permeating dislocations showed any high

amount of Si. Any such variation would have to occur during growth of the epitaxy. The problem was not apparent in the (100) standard as verified by both the chemical analysis and earlier Hall measurements.

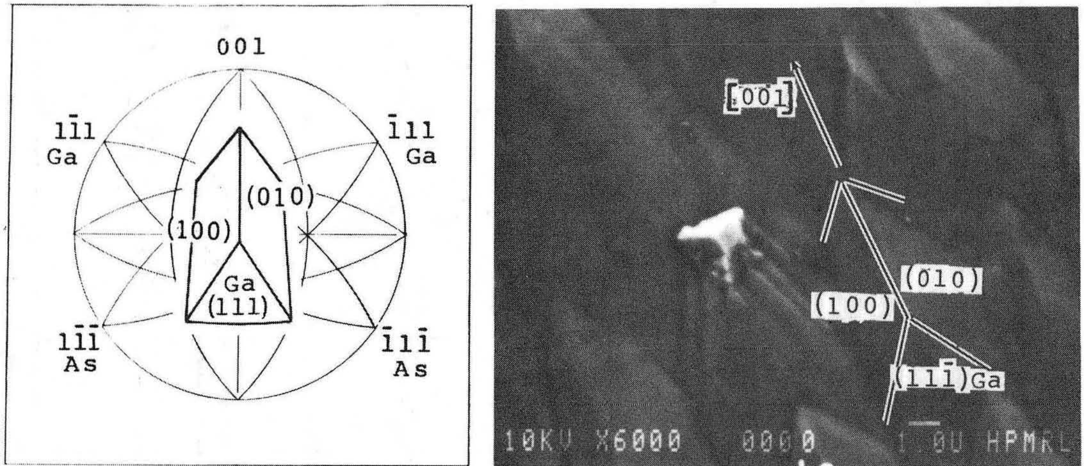

XBB 860-9598

Figure 16

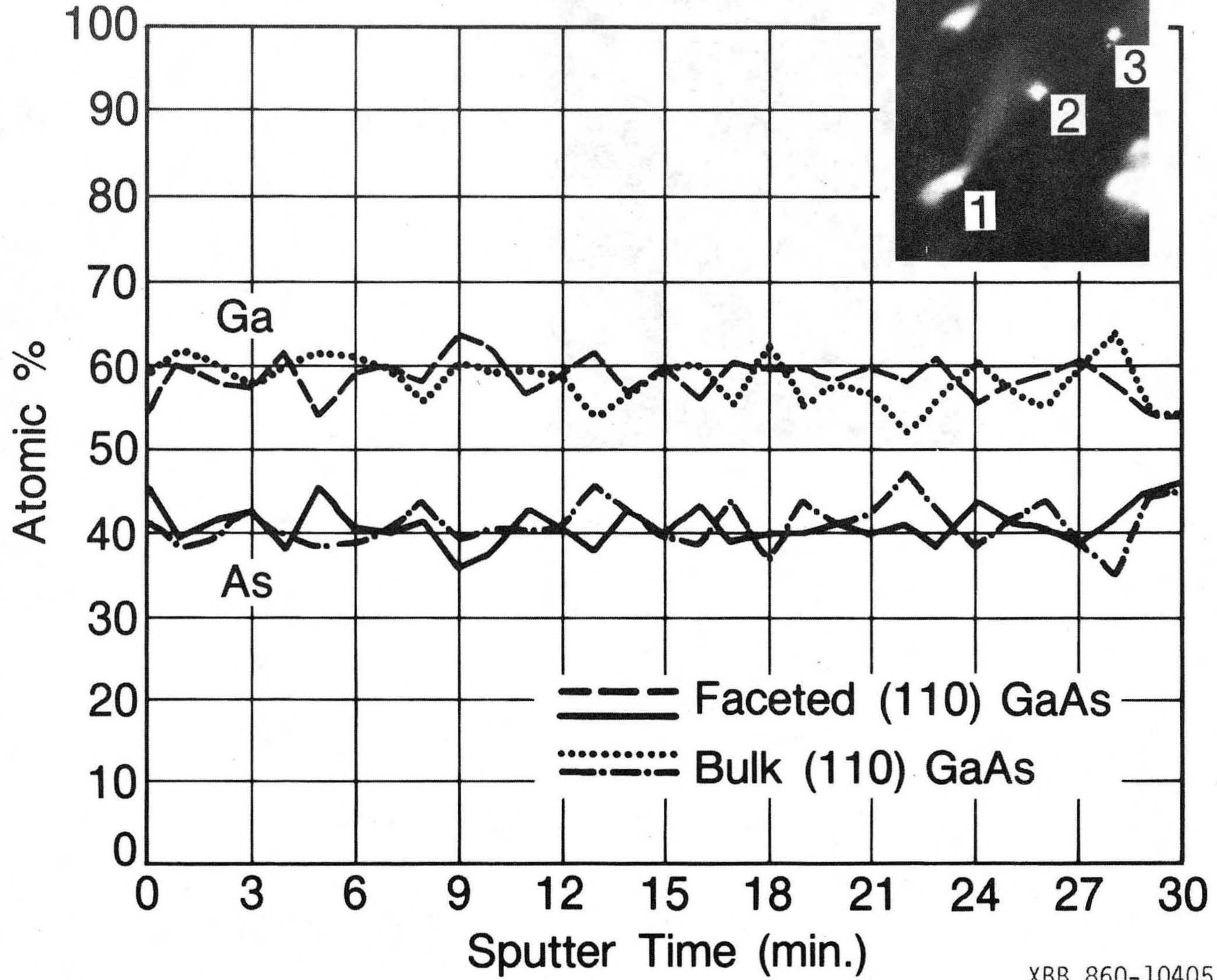

Figure 17

V. EXAMINATION OF INITIAL FACET FORMATION AND EFFECT OF SUBSTRATE ANGLING

In order to better understand the kinetics and thermodynamics of facet growth on (110) GaAs, the initial growth and facet formation on the cleaned and prepared GaAs (110) substrate was examined. The initial layers were studied in comparison to the first layers of a (100) GaAs epitaxy. The progressive formation of the previously defined facets was the main focus of the investigation. A model of the facet formation was a necessary step toward the total elimination of these surface defects. This was based on kinetic considerations of initial atomic chemisorption and anion/cation configuration. A thermodynamic model based on the surface energies of the various crystal planes of GaAs was not possible, as that information is not presently available.

Separate runs of 100 Å, 700 Å, and 1500 Å of epitaxy were grown on the (110) and (100) GaAs substrates. Figure 18 shows the SEM micrographs of these layers at both 2600X (left) and 26,000X (right) magnification. By 100 Å of growth, the larger magnification shows that surface defects had initiated and were not from the substrate. In the 700 Å film, facet progression shows that the (110) GaAs surface was replete with defects that had taken on the analyzed facet shape. The micrographs of the 1500 Å epitaxy show that the facets had continued to grow and had overlapped other facets in the process. The dark circles at the tip of the facets seen in higher magnification are due to a difference in SEM contrast resulting from a contaminating silver

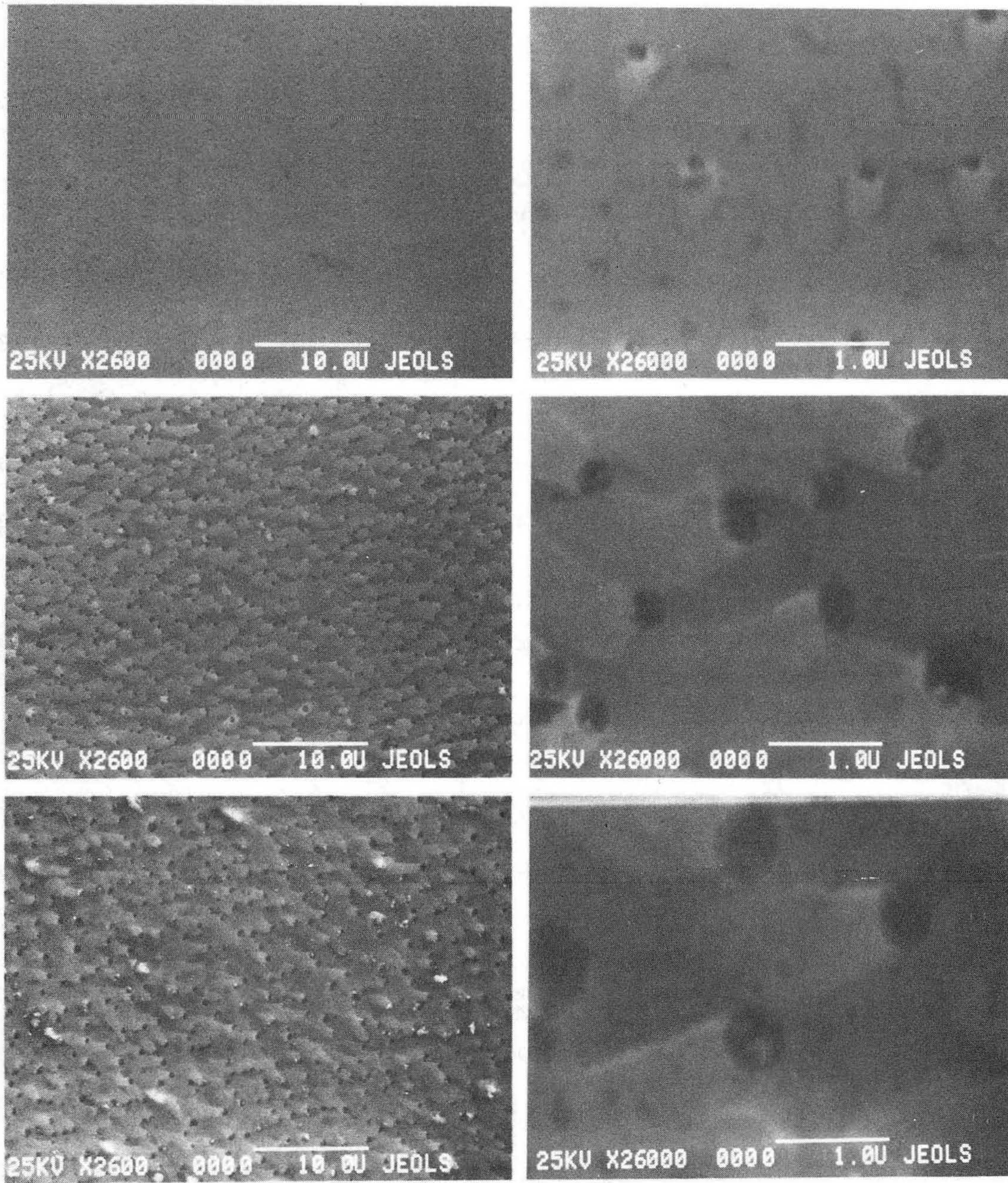

XBB 860-9600

Figure 18

paste film used to secure the SEM sample and are not pits or due to an unusual GaAs feature. The (100) GaAs standard showed smooth, shiny epitaxy with each growth. No facets or unusual MBE defects were observed.

For epitaxial growth of semiconductors, a generally verified phenomenon is that the creation of a larger number of ledges on the substrate surface helps to initiate smooth epitaxy growth [39,40]. This is accomplished by slightly angling the substrate away form the primary axis. The geometrically required surface ledges may provide the sites for initiation of a lateral growth process on a particular surface of a crystal. These natural ledges, in the absence of 2-dimensional nucleation, may decrease in density during the growth process as surface coverage increases. Therefore, it is worth considering a dislocation ledge mechanism which would provide a constant source of ledges during the epitaxy growth. Such ledges on the substrate surface will be present, connecting screw dislocations of opposite sign. Any dislocation type which produces a shear displacement in the z direction across the xy plane will be connected with a screw dislocation of the opposite sign some distance away by a ledge of material inbetween them. Five out of the six available Burger's vectors have either a pure screw component (one) or a partial screw component (four) when the dislocation intersects with the (110) surface.

Substrates were obtained that were angled 6° off-axis from the (110) orientation. The four semi-insulating off-axis substrate orientations were: 6° towards (010), 6° towards (100), 6° towards (111) and

6° towards $(11\bar{1})$. These directions can be seen in the stereographic projection of Figure 19. The specific orientations were verified by Laue x-ray diffraction. Besides increasing the density of natural ledges available on the off-axis (110) GaAs substrate, the exposed ledges were also of different chemical nature. The tilting of the substrate towards {100} creates non-polar ledges as visualized in the cross-section schematic of Figure 20. The pairs of As-Ga are present at each ledge, leaving no one type of anion or cation in predominance. Also shown is the difference in tilting the substrate towards the opposite {111} planes. The tilting toward one (111) creates polar ledges which have all As or all Ga atoms along the ledges, while tilting towards an opposite direction of the $(11\bar{1})$ creates polar surface ledges exposing all Ga or As, respectively. With an angling of 6°, a step or ledge on the (110) GaAs surface is created approximately every eight Ga-Ga planes. A slightly greater angle would result in the creation of a (771) GaAs surface which is thermodynamically of high energy. A lower angle approaching 2° off-axis would result in the faceted growth described in this research. Thus, optimal angles considered were between 4-6° off of the (110) orientation.

The novel CBED technique described in Chapter 3 to differentiate between As and Ga planes in GaAs material was utilized once again to determine the nature of the ledges for the off-axis substrates angled 6° toward (111) and 6° toward $(11\bar{1})$. The same pairs of diffracted beams were utilized along with the same reference stereographic projection. The results showed that the tilting of the substrate 6°

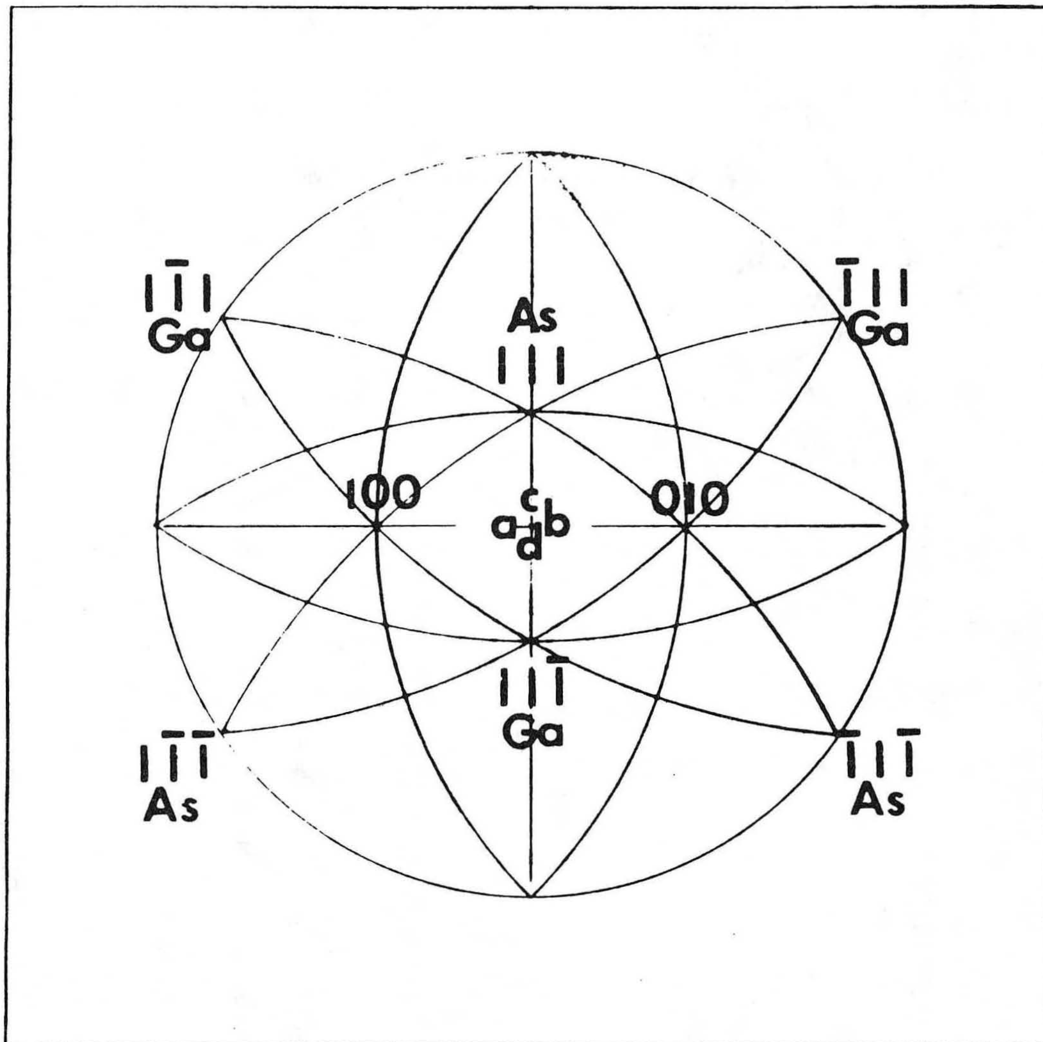

XBL 8611-4617

Figure 19

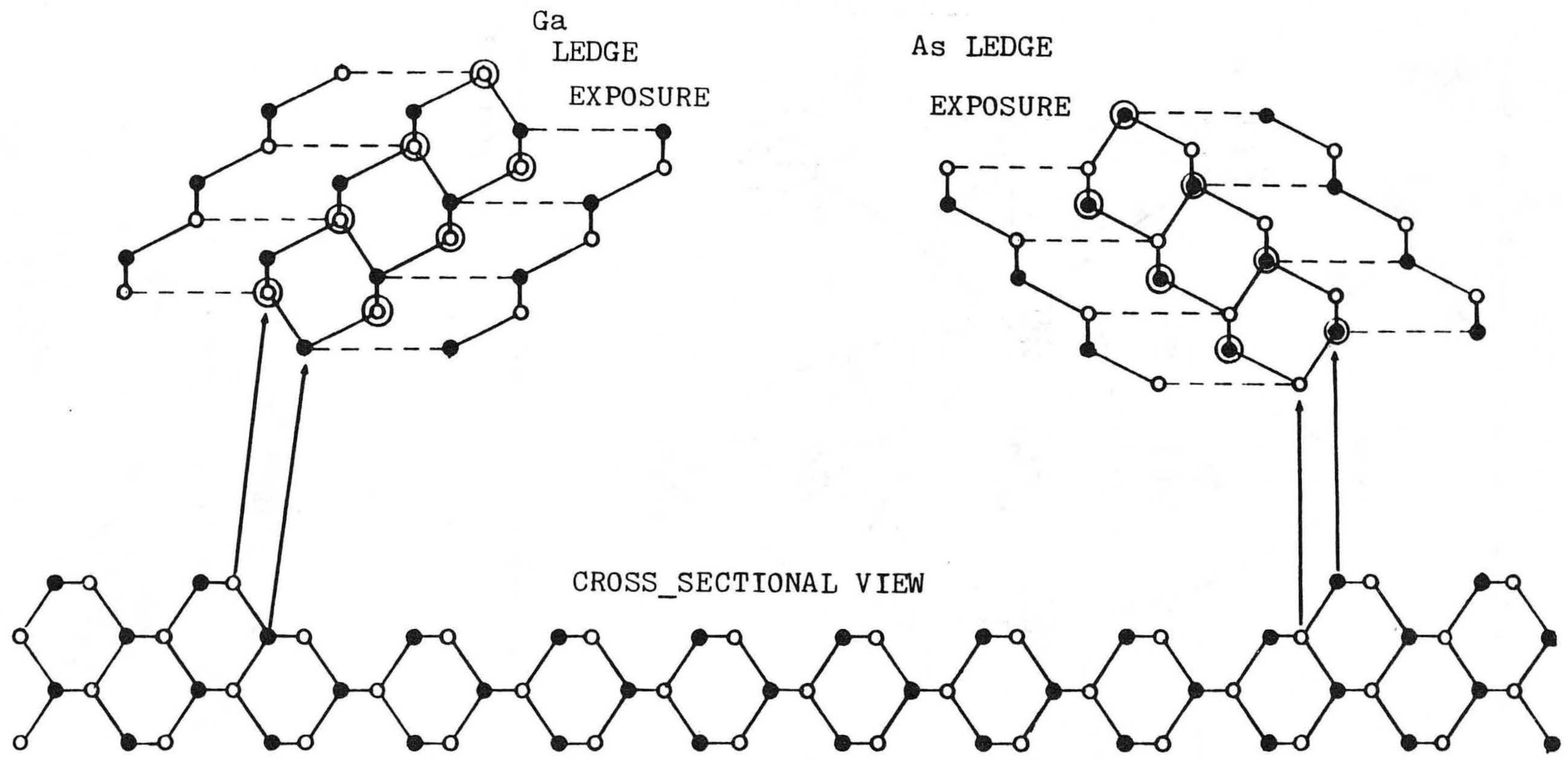

Figure 20

towards (111)As created all As ledges. By symmetry and by confirmation with the CBED technique, the off-axis substrate tilted 6° toward $(11\bar{1})$Ga exposed ledges of all Ga in nature.

MBE layers of 100 Å, 700 Å and 1500 Å were grown on each angled substrate and examined with the SEM. Figure 21 shows each thickness of epitaxy on the substrate tilted 6° towards (010) from the (110). Shown are micrographs at 2600X (left) and 26,000X (right) of the resulting epitaxy. The films show that facet initiation begins at less than or equal to 100 Å of growth. The surface coverage of facets has been completed by 700 Å of growth as shown in the middle set of the same figure. The growth pattern of the facets progressed in the same manner as the (110) epitaxy in that the defects continued to grow and overlap one another as shown in the bottom set of micrographs in Figure 21. The facets appear the same as the near axis (110) epitaxy growth. Growth on the substrate angled toward the opposite 100 , or 6° toward (100), is shown in the SEM micrographs of Figure 22. The top pair of 2600X (left) and 26,000X (right) shows the 100 Å film which had, once again, begun to facet at less than or equal to that thickness of epitaxy. The middle pair of micrographs show the 700 Å GaAs film which shows the surface replete with faceted sites. Just as the previous substrates, the 1500 Å film showed no improvement in facet retardation. The facet appearance was somewhat different for the films grown on substrates angled 6° toward (111)As. Nevertheless, defects appeared by 100 Å and continued to develop as epitaxy thickness increased as shown in Figure 23. For the films grown on the substrate

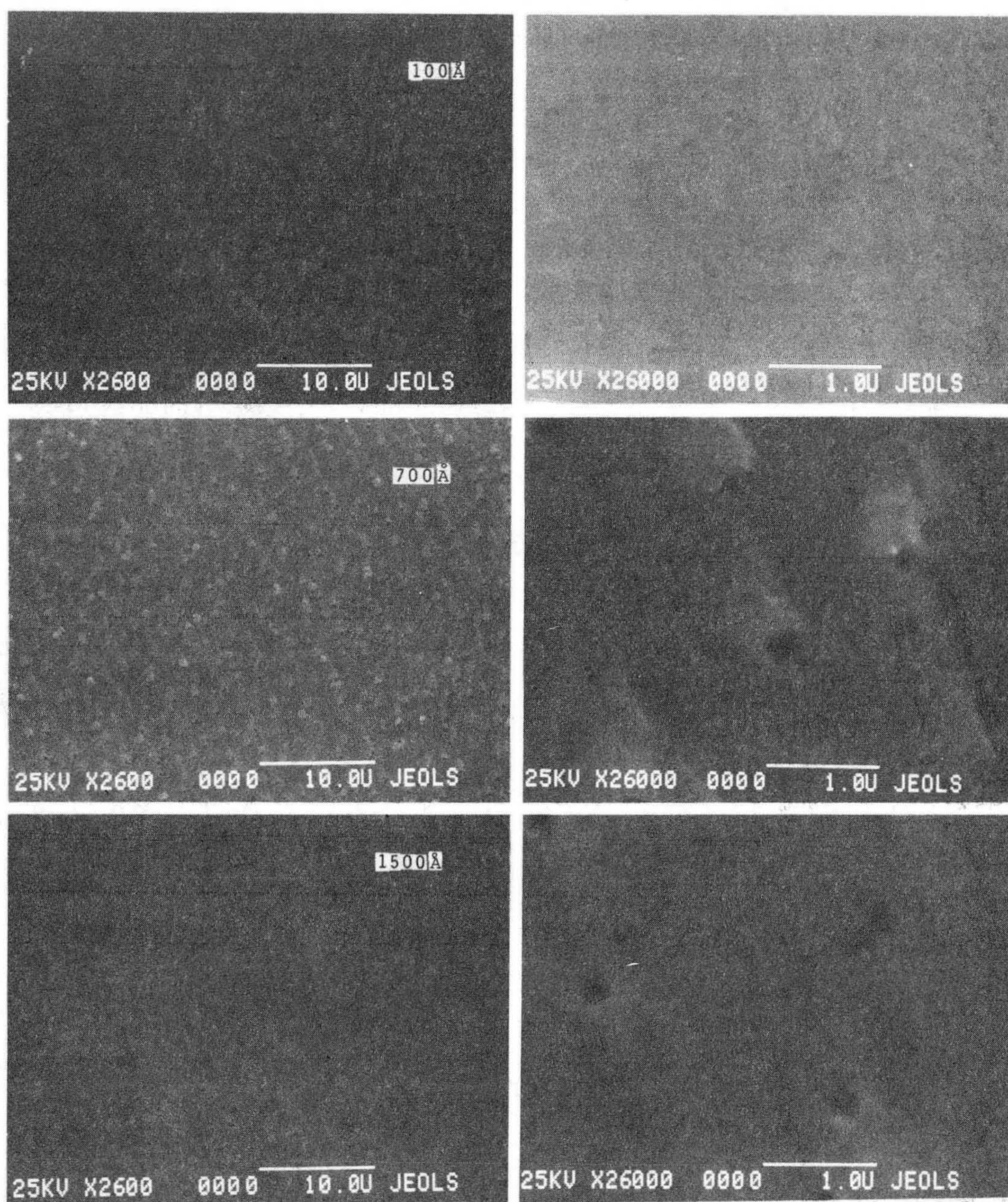

XBB 860-8817

Figure 21

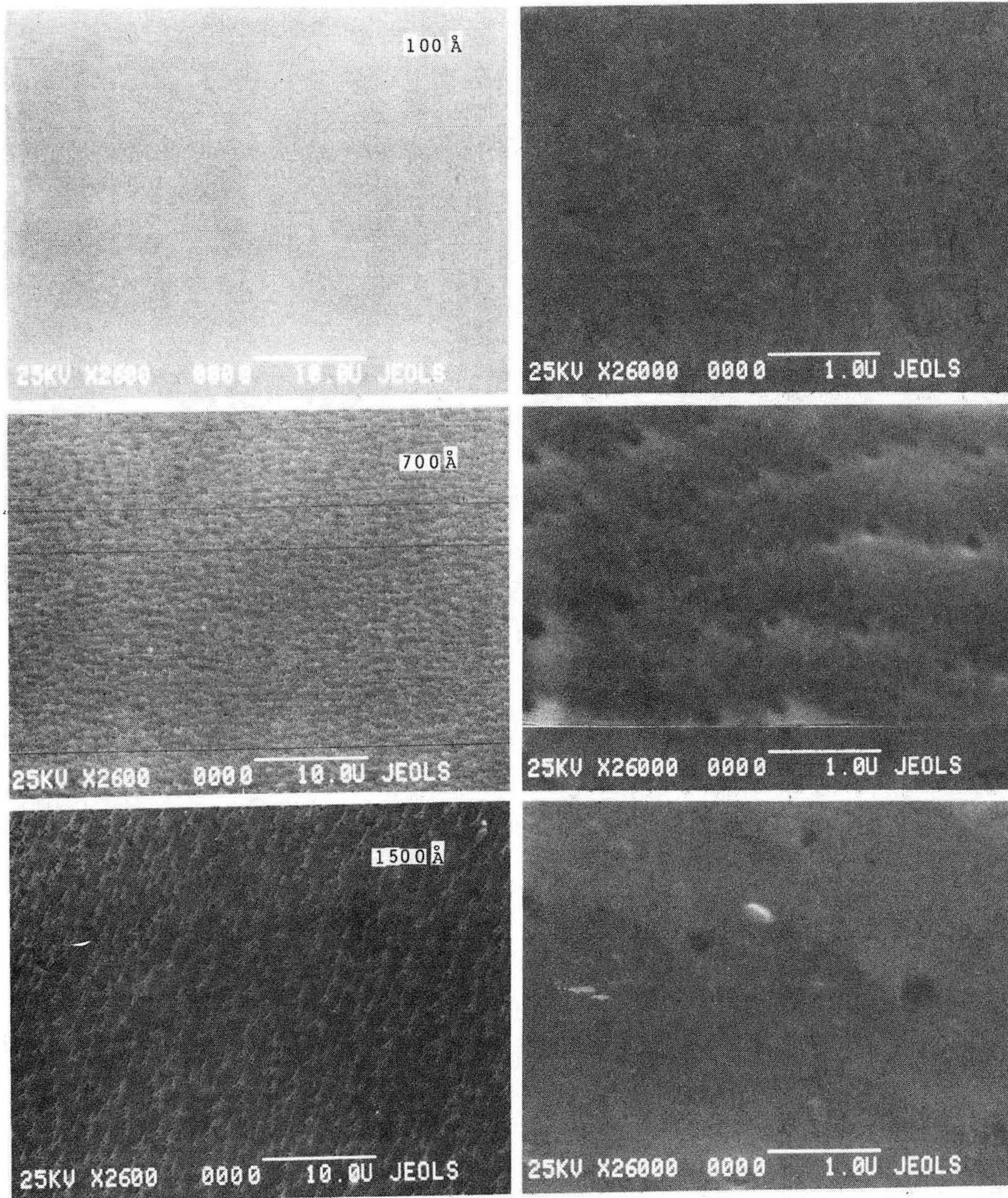

XBB 860-8815

Figure 22

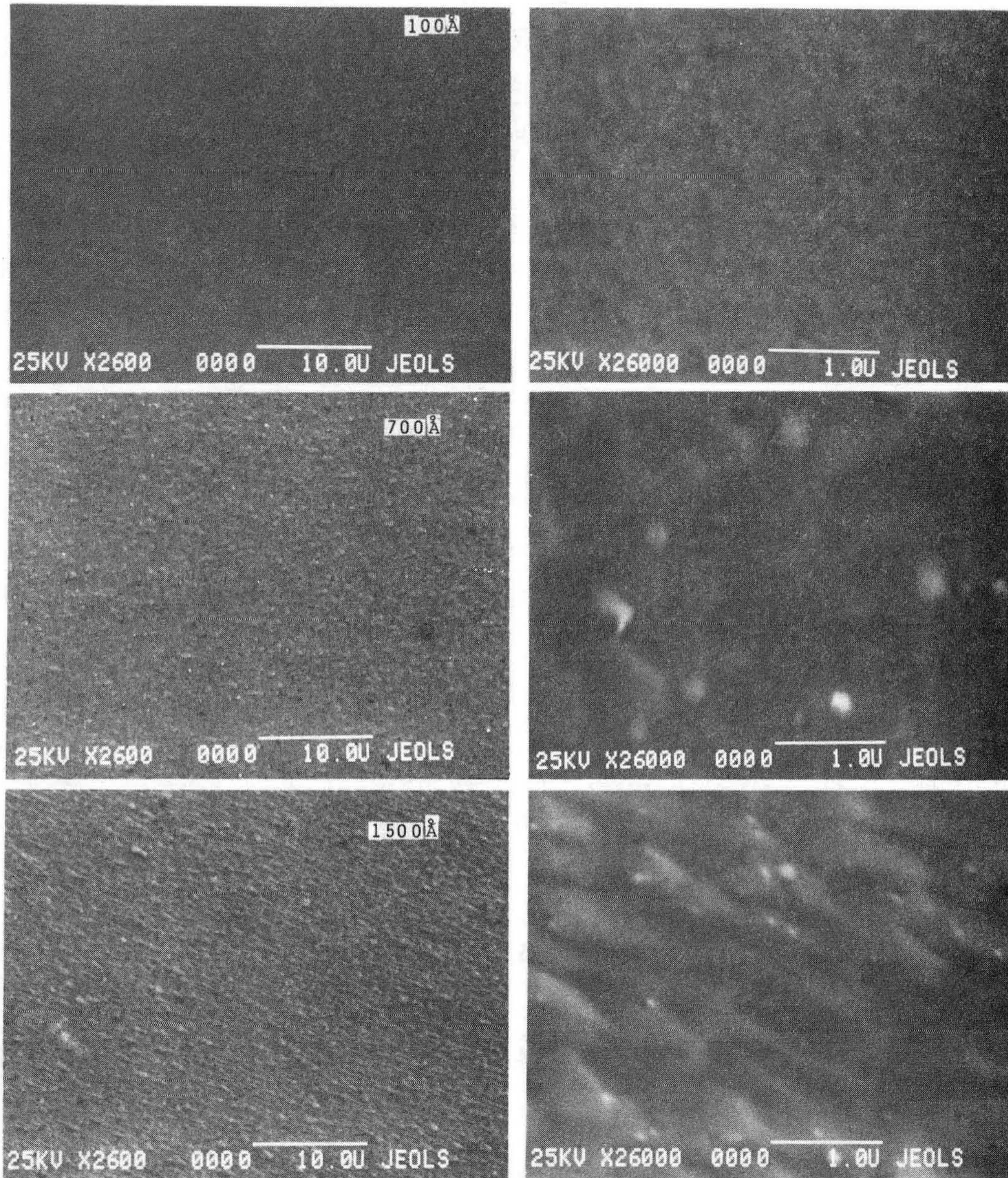

XBB 860-8818

Figure 23

angled 6° towards $(11\bar{1})$Ga, however, there was a startling difference in epitaxy morphology. The resulting films were defect free even at 1500 Å as shown in Figure 24. No facets were observed for the varying thicknesses and the films had the same smooth, shiny appearance as the (100) standards. The typical appearance of the 1 micron (110) GaAs epitaxy grown on the successful 6° off-axis substrate is shown in the SEM image of Figure 25. TEM further verified the facet free character of the successful (110) film as shown in Figure 26. The large plan-view area exposed shows no defects, although bend contours are visible throughout the image. These encouraging results of the off-axis (110) films demanded further attention.

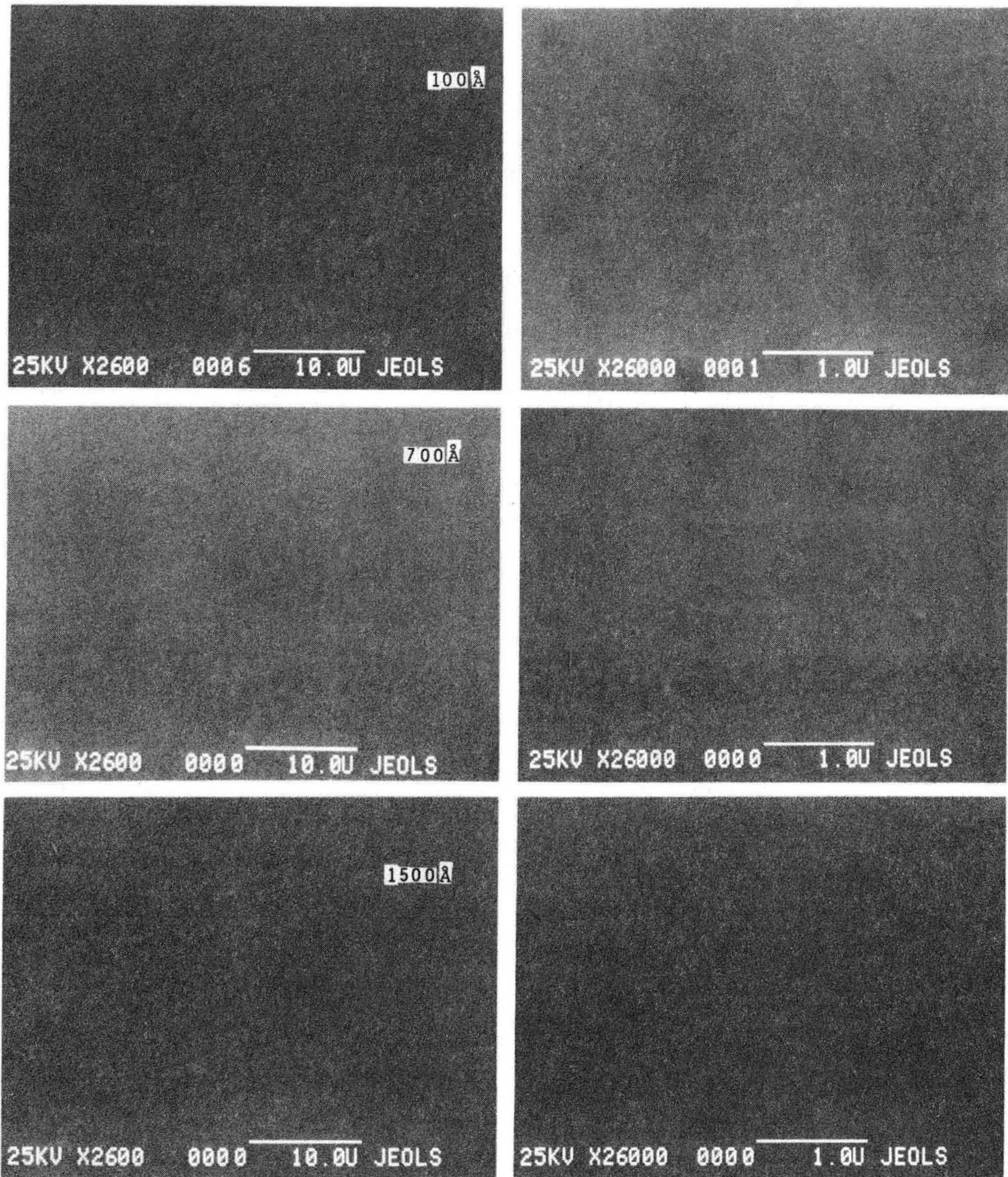

XBB 860-8816

Figure 24

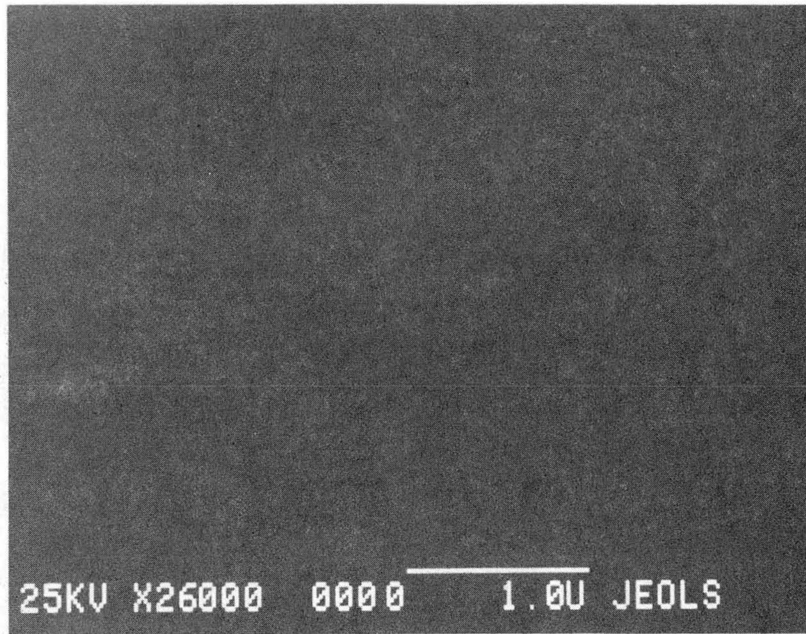

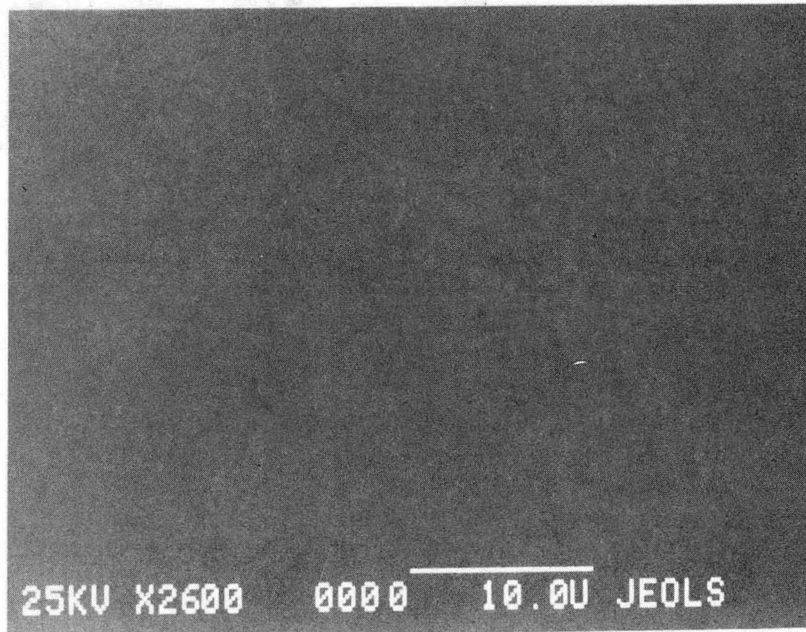

XBB 860-9601

Figure 25

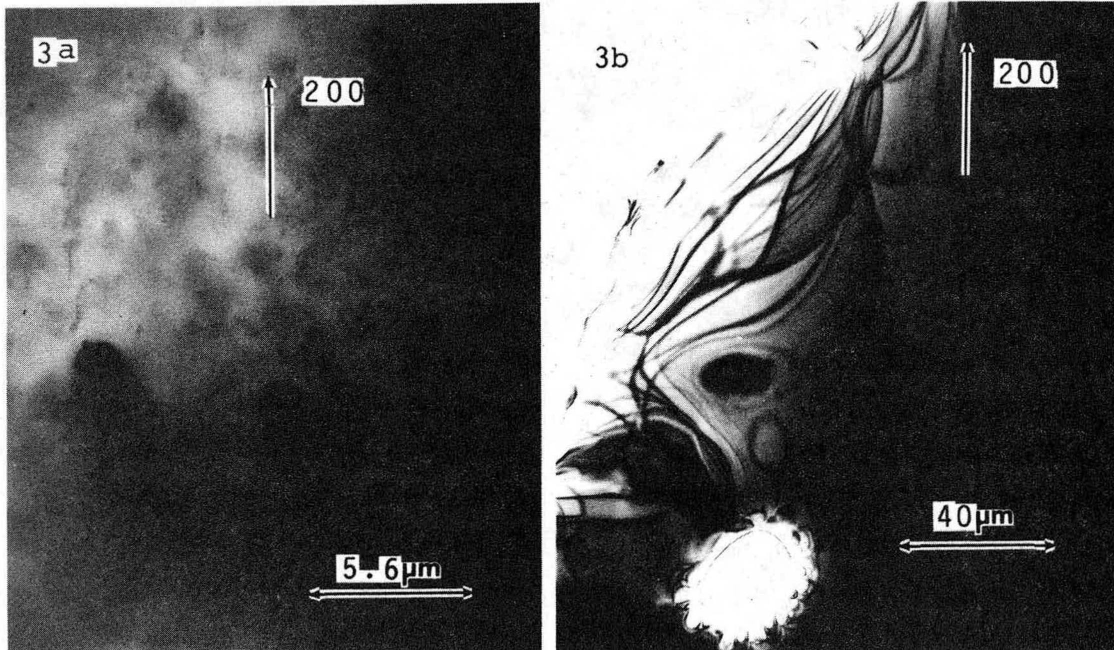

XBB 860-8819

Figure 26

VI. ELECTRICAL AND OPTICAL CHARACTERISTICS OF SUCCESSFUL (110) GaAs/GaAs AND (110) AlGaAs/GaAs

The true value of an epitaxy depends on the quality of the material obtained with electrical and optical characteristics that satisfy specific criteria of a potential user. For example, while certain deep level centers in GaAs may be beneficial for specific applications (e.g. the mid-gap EL2 level desired for ensuring semi-insulating GaAs substrates [41]), they are generally undesirable in GaAs epitaxy because they act as carrier traps [42] which lead to poorer device performance. Variable temperature Hall effect, liquid He PL, DLTS, and CV characteristics were obtained for the non-faceted (110) GaAs as compared to the (100) GaAs of known device quality. This provided a basis for the assessment of the first successful MBE GaAs growths on (110) substrates. In addition, AlGaAs/GaAs superlattices were also characterized for Al mole fraction content.

The variable temperature Hall effect data for the 1 micron non-faceted (110) GaAs film, the faceted (110) epitaxy, and the (100) GaAs standard is shown in Figure 27. The three films were grown under the same MBE conditions, the difference between the (110) films being the 6° off-axis substrate orientation of the successful epitaxy. The carrier concentration as a function of temperature was compared for the different layers. The carrier type and concentration of the non-faceted (110) GaAs epitaxy coincided well with the (100) GaAs device quality standard material. The room temperature Si donor concentration was in the range of the targeted mid $10^{15}/cm^3$. This result was a

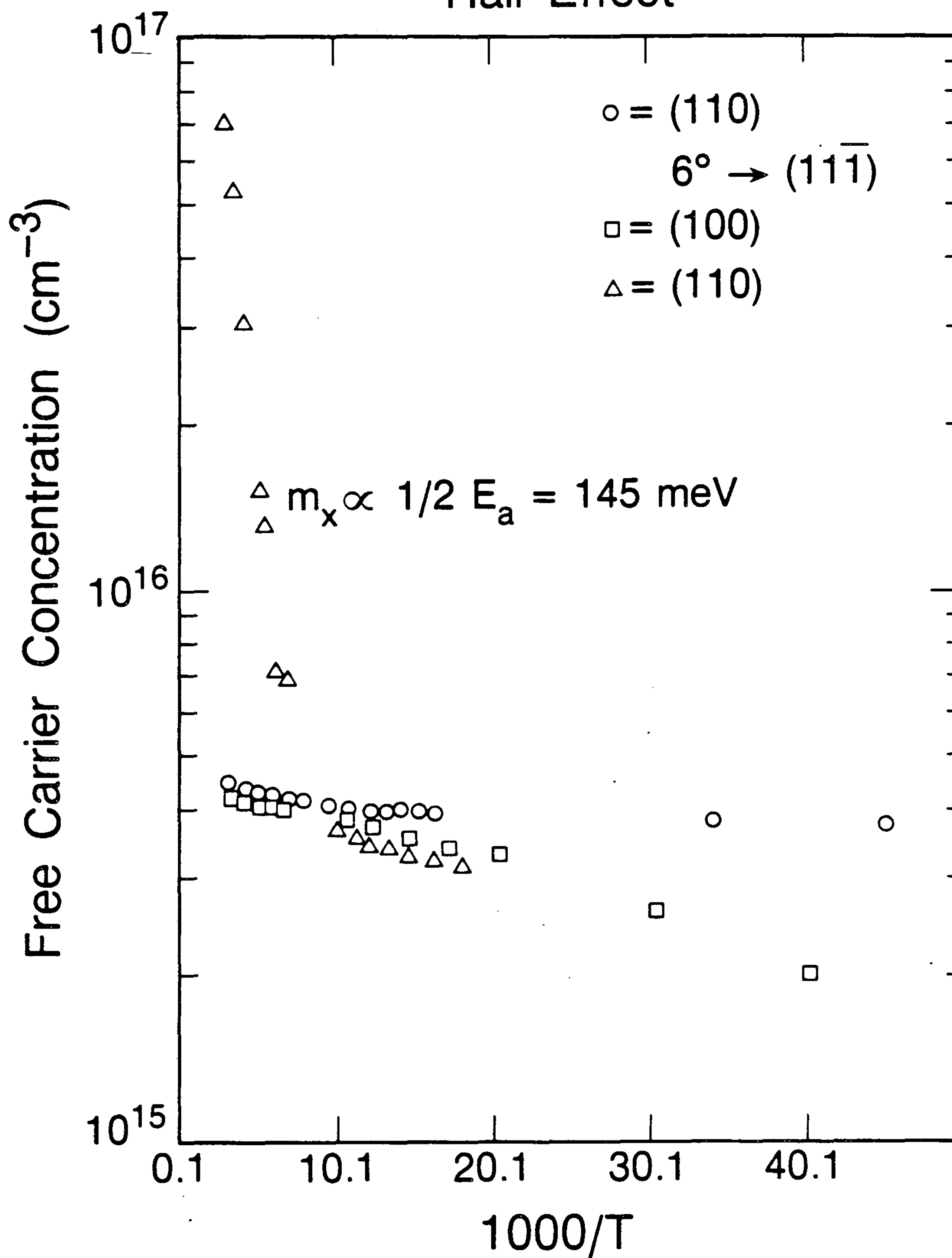

Figure 27

great improvement over the unpredictable doping type and behavior of the faceted (110) GaAs material described in Chapter 2. The characteristic carrier freezeout with an activation energy of ~145 meV was not found in the non-faceted (110) GaAs material. Figure 28 shows the Hall mobility of the carriers as a function of temperature for the same three films. Nearly identical excellent room temperature mobilities of ~5700 cm^2/V-sec were achieved for the non-faceted (110) and (100) standard GaAs. It is clear that the mobility of the non-faceted (110) GaAs compared favorably to that of the (100) GaAs standard epitaxy whereas the mobility of the faceted (110) film is reduced by ~2 orders of magnitude.

Liquid He PL response for 1μm films of the (110) off-axis substrate, the (110) off-axis epitaxy (non-faceted), the (100) epitaxy, and the (110) faceted epitaxy are shown in Figure 29. The PL response of the successful off-axis (110) GaAs substrate is shown in order to eliminate background data from that source. Luminescence of the faceted (110) material showed a small exciton, neutral acceptor transition (x,A°) peak at 1.512 eV. This is indicative of poor quality material as previously explained. The dominance of the neutral carbon acceptor emissions near 1.490 eV for the faceted (110) GaAs epitaxy is indicative of the high degree of acceptor compensation also observed in the Hall data for that film. The PL spectra for the successfully angled substrate showed an extremely weak bound exciton transition (x,D° or A°) peak as was expected for semi-insulating GaAs. The non-faceted (110) epitaxy grown on the same type of successful substrate

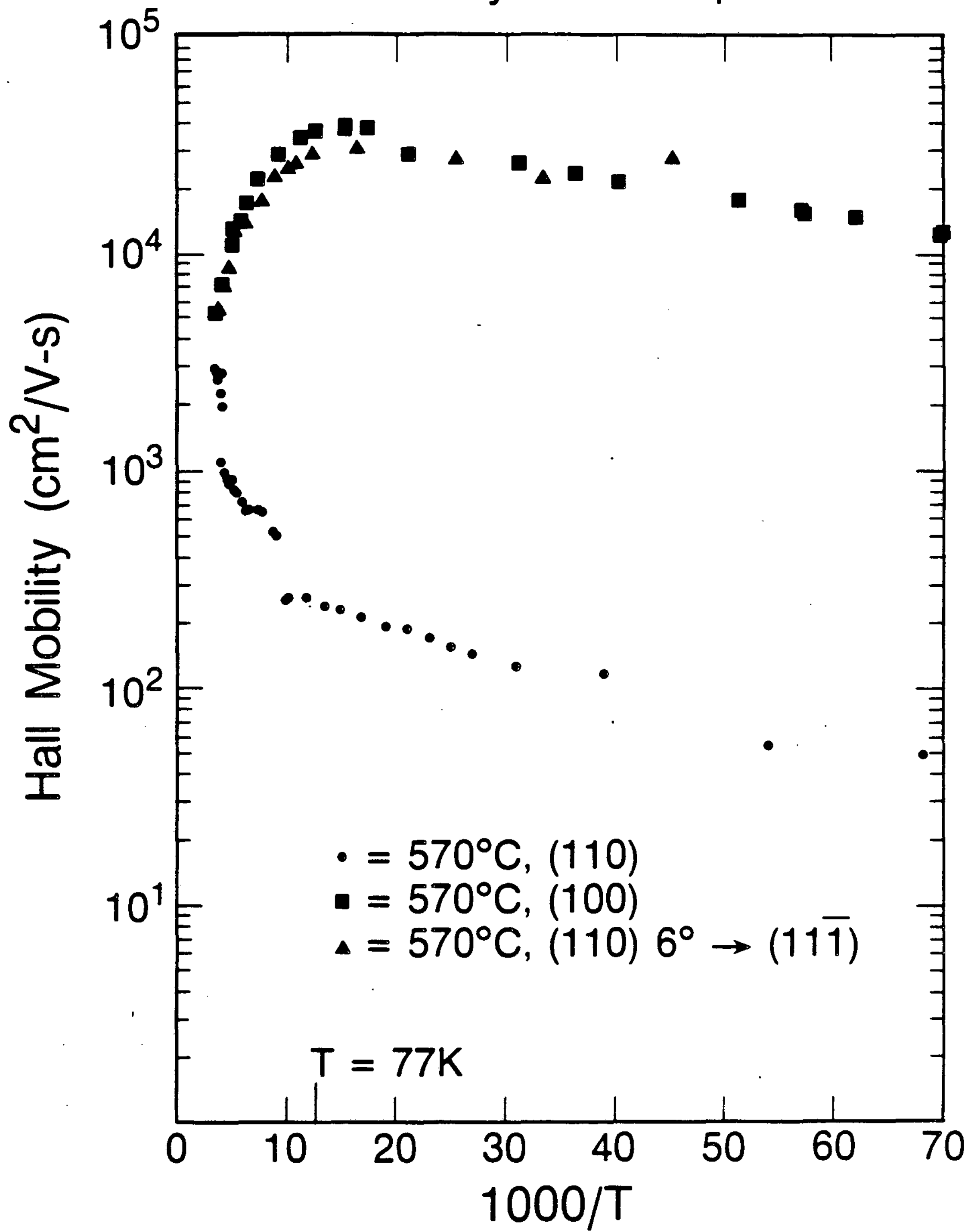

XBL 8611-4616A

Figure 28

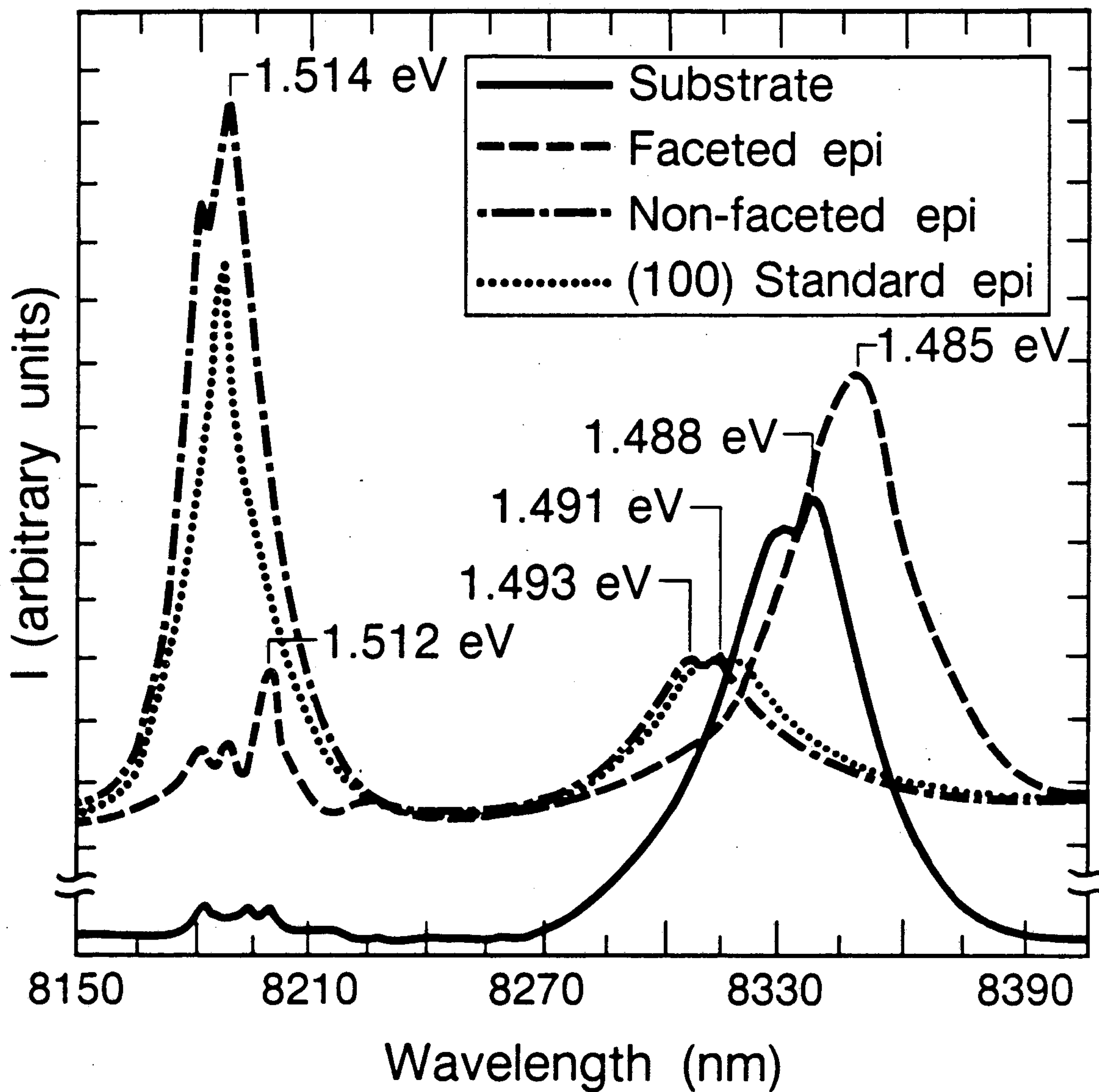

Figure 29

angled 6° toward $(11\bar{1})$Ga indicated a strong neutral donor, bound exciton transition (x,D°) peak at 1.514 eV dominating the spectrum. The observed shift in the bound exciton peak from 1.512 eV to 1.514 eV suggested that the Si dopant had shifted from a preferred acceptor site in the faceted (110) GaAs to a predominately donor site in the non-faceted (110) GaAs [43], a fact supported by the Hall effect data. The bound exciton peak in the non-faceted (110) epitaxy is favorably compared to the small neutral carbon acceptor transition (D°,A°) peak at 1.490 eV of the same spectrum. PL of the (100) GaAs standard showed comparable luminescence output to the non-faceted (110) GaAs film. The results are indicative of device quality material for both the (100) and non-faceted (110) GaAs epitaxy [44,45].

Differential analysis of the CV measurements for the non-faceted (110) GaAs and the (100) GaAs standard are shown in Figure 30. No reliable contacts could be made on the faceted (110) epitaxy. The forward and reverse bias characteristics of the two films are nearly identical and are of excellent quality. The doping behavior as a function of depth for the non-faceted (110) films are uniform and verified the carrier concentrations observed in the Hall data. The slight decrease of Si dopant content in the (100) epitaxy as a function of depth is speculated to be a result of Si diffusion into the substrate during growth or Schottky/ohmic contact processing. The (100) face of GaAs is the least close-packed and may contribute to enhanced diffusion in this orientation [46]. CV analysis of a (110) GaAs MESFET grown on the successful (110) substrate indicated the n^+ MESFET channel

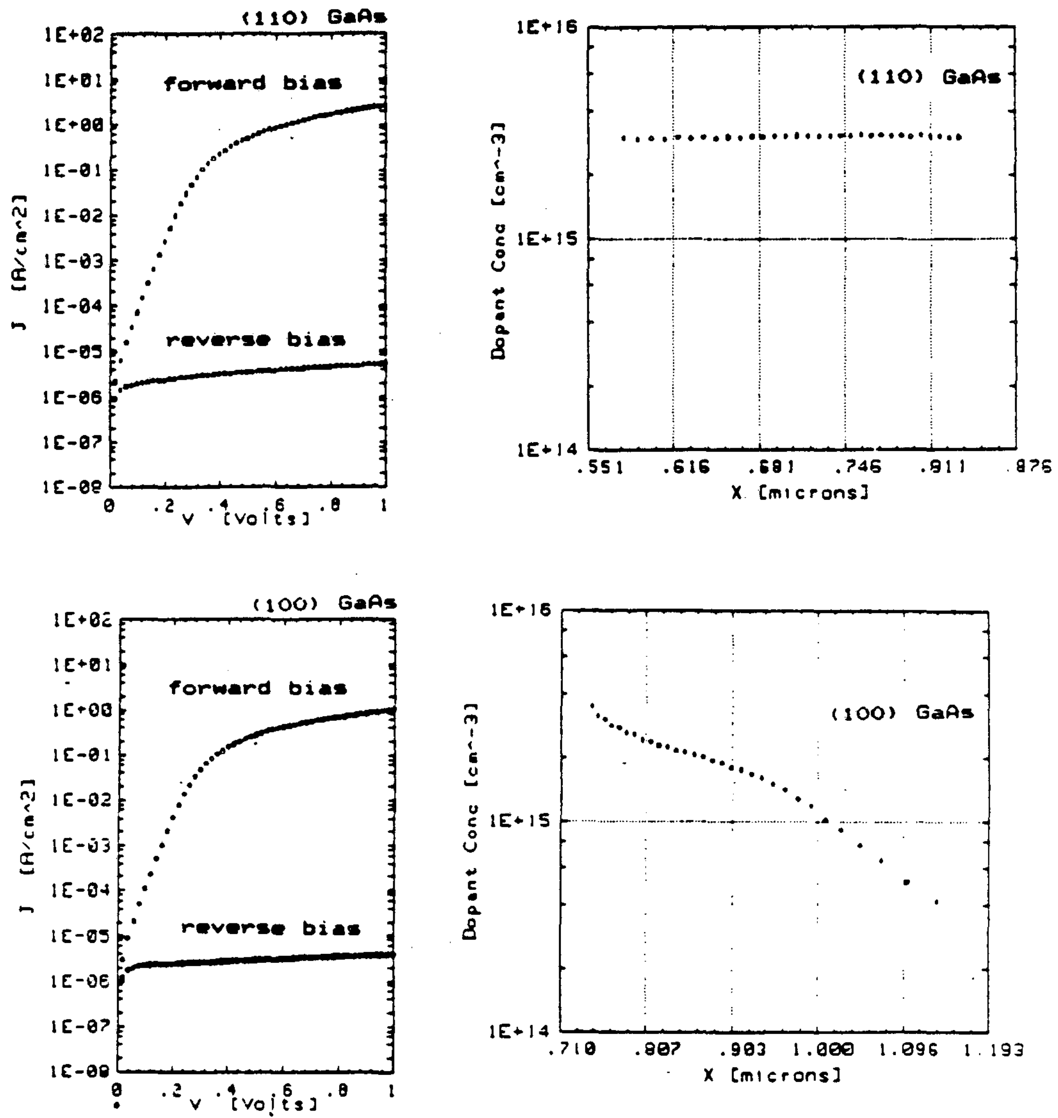

Figure 30

had the intentional doping of ($2x10^{18}/cm^3$) with the underlying n-type layer doped with the desired ($3x10^{17}/cm^3$). Further device testing of that MESFET is underway at the Varian III-V Device Center, Santa Clara, CA.

DLTS data of the non-faceted (110) GaAs angled 6° toward $(11\bar{1})$Ga showed the well-known M1, M3 and M5 levels [47] in the 10^{12}-$10^{13}/cm^3$ range. The concentrations of these deep levels which are associated with residual carbon and oxygen related contamination compare well with the simultaneously grown (100) standard epitaxy as shown in Table II. DLTS of the faceted (110) GaAs is planned to verify the deep donor level of (E_C-.29 eV) observed in all faceted material.

A (110) superlattice structure of alternating GaAs/AlGaAs layers was grown in the configuration of Figure 31. It was a necessary step in proving the device quality of the non-faceted (110) GaAs films and represents an exciting new direction of scientific exploration. No (110) GaAs/AlGaAs superlattices have been grown up to now due to the previously unattainable high quality epitaxy required. Room temperature photoluminescence of the AlGaAs/GaAs superlattice indicated an Al mole fraction of 28%. Cross-sectionalTEM results showed that the desired layer thicknesses were achieved.

TABLE II: DLTS MEASUREMENTS

	(110) GaAs	(110) GaAs	TEMP (K)
M1	8 X 10E13/cm3	1.6 X 10E13/cm3	110
M3	3 X 10E12/cm3	1.0 X 10E13/cm3	160
M4	4 X 10E13/cm3	2.0 X 10E13/cm3	210

10Å GaAs

300Å AlGaAs

15Å GaAs

300Å AlGaAs

25Å GaAs

300Å AlGaAs

50Å GaAs

300Å AlGaAs

100Å GaAs

300Å AlGaAs

2000Å undoped GaAs

SUBSTRATE

Figure 31

VII. KINETIC THEORY OF FACET FORMATION AND ELIMINATION ON (110) GaAs

Both kinetic and thermodynamic considerations of the surface faceting phenomenon on (110) GaAs were studied in forming a theory of the observed formation and elimination of these defects. For FCC metals, faceting may occur when crystal growth from the melt takes place because the thermodynamics of the system dictates that high energy planes of the crystal should not be exposed. At least one low index plane is typically exposed as a result of the faceting. For the GaAs crystal which can be thought of as two interlocking FCC lattices, it is difficult to speculate on the thermodynamics of the epitaxy growth due to the complexity of determining the relative surface energies of different crystal planes in the ultra-high vacuum environment. Experimental information concerning these values does not exist yet. Several experimental observations, however, indicated that a kinetic approach would be fruitful in the attempt to eliminate facet formation on the (110) GaAs surface. One indication was that the growth rate of the (110) epitaxy was proportional to the rate of growth of the facets. The slower the growth rate, the slower the facets formed.

The epitaxy growth itself is not a kinetically simple process. For the (110) surface, an incoming Ga atom must first combine with an incoming As atom such that the pair can form two bonds to the surface as shown in Figure 32. A qualitative prediction suggests that the pair is unlikely to approach the surface together in the proper configuration as the As_4 species must first break up into two As_2

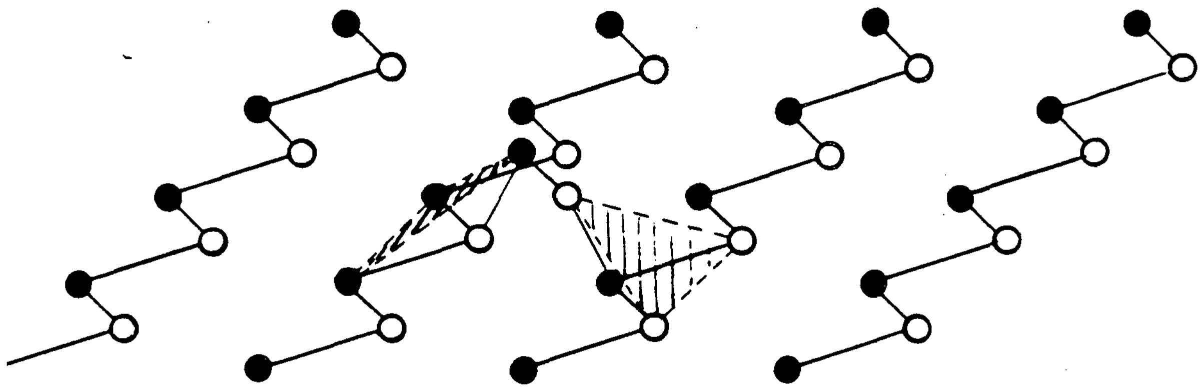

Figure 32

molecules and, finally, into four As atoms on the GaAs surface. Physisorption of the Ga and As species is rapid, but even then the As species has a high desorption rate due to its low sticking coefficient [1]. Thus, one may expect that a slower growth rate would enhance the proper chemisorption of the molecular species and reduce the amount of surface faceting. Although this was not the case, a kinetic approach was still a viable one when the non-polar surface is accounted for, as follows. Aside from a ledge or defect, there is no energetically favorable site that is readily apparent to the incoming molecular beams on the theoretically flat [48], non-polar surface. The (110) surface requires a correct configuration of the two atoms (Ga and As) to form the next monolayer [49]. Despite the amount of time available to chemisorb onto the (110) surface, the impinging atoms may indeed chemisorb sporadically along the non-polar surface to form many new monolayer sites. This conforms with the observed defects at less than 100 Å of growth. There, the surface was not completely covered with visible facet defects. These surface perturbations continue to form the atomic site basis for the new monolayer while, at the same time, offering the incoming Ga, As, and Si atoms a surface available for yet a second monolayer formation. Thus, both two and three dimensional growth is possible on the growing epitaxy [50]. Eventually, the nucleated sites of the facets begin to form the distinctive polygonal shape and overlap each other as the GaAs epitaxy grows. Thus, the relative rate of facet growth is consistent with the varying growth rate data of Chapter 2.

The introduction of ledges on the substrate can provide preferred sites for initiation of two dimensional growth which is inherent in the MBE process [21,50]. The results of the substrate angling experiments, however, prove that the nature of the ledges is decisive for growth on the non-polar (110) surface. The introduction of non-polar ledges did not improve the surface morphology over that of the perfect (110) surface. When a Ga and As pair bond to the (110) surface, Figure 32 shows that both types of {111} planes are then exposed on the epitaxy with respect to the incoming molecular species. A kinetic approach suggests that the As-exposed (111) tends to be unstable and may desorb in the ultra-high vacuum environment. For MBE growth to be As-stable, Arthur [51] reported that nearly 60% of the surface site occupancy is by As. His results showed that Ga-stable surface requirements were far less stringent. Many other early MBE studies have reported the difficulty of obtaining an As rich surface for MBE growth [52,53]. Once the As desorbs from the configuration of Figure 32, a non-polar surface is once again exposed. The stable $(11\bar{1})$Ga surface, however, can serve as a basis for further chemisorption of the incoming molecular beams of Ga and As species. As a result, the exposed Ga-rich $(11\bar{1})$, as verified with the novel application of the CBED technique, continues to provide the stable growth surface. Facets begin to form from the fast growing $(11\bar{1})$Ga back surface, with sides of {100} filling in. These are thermodynamically favored planes to expose. For the thin layer growths, it is seen that the facets continue to form until the surface coverage is complete. The {100} sides and $(11\bar{1})$Ga back planes then begin to overlap.

From the above discussion, it is clear that the introduction of non-polar ledges on the substrate surface would not improve the GaAs epitaxy. The neutral GaAs surface and ledges obtained when angling the (110) substrate 6° towards $\{100\}$ still allows the exposure of the stable $(11\bar{1})$Ga vs. unstable (111)As sites. The exposure of As-rich ledges when angling the surface 6° toward (111)As resulted in the formation of facets because of the unstable nature of the As planes. Desorption of the As atoms leave behind non-polar ledges. Only the exposure of stable Ga ledges provides the necessary nucleation sites for the layer by layer, planar growth of the (110) MBE GaAs. Because the incoming As atom finds four Ga atoms in place on the ledged (110) surface, it will tend to chemisorb at that available site. Recent work of Brigans confirms early speculations that the As species incorporation is the necessary initial step for planar growth in ultra-high vacuum [54]. The ledge provides the thermodynamically favorable site, as well, to begin formation of the next layer of epitaxy. For (100) MBE growth, the ledges may well promote a lateral growth mechanism [50]. For (110) MBE growth, the natural step ledges did not provide a site for smooth lateral growth. Facets resulted unless a large number of Ga ledges were provided on the substrate surface. For the facet free case, there are two alternatives: (1) the ledges provide stabilizing sites for lateral epitaxy growth combined with 2-dimensional nucleation throughout the growth process or, (2) the abundance of screw dislocation pairs provides the ledges necessary to promote lateral growth without the need for two-dimensional nucleation. In

either case, by providing the facet initiation sites as a natural substrate feature, the facet formation is avoided and a smooth, high quality GaAs epitaxy on the (110) surface results.

As discussed in Chapter 4 and above, the role of screw dislocations may play an important role in the continuation of surface ledges in the epitaxy growth process. If screw dislocations are present on the non-angled substrate surface, pairs of opposite sign screw dislocations will result in either (1) Ga ledges, (2) As ledges, and (3) non-polar ledges. However, the tilting will result in the screw dislocation pairs being connected in a way which produces predominantly one type of ledge. The geometry of the screw dislocation pairs ensures that a constant excess length per unit area of Ga or As (or non-polar) ledges is maintained. In view of the above epitaxy growth considerations, the screw dislocation pair ledges which provide As fronts would be annihilated or cancelled out by the spreading Ga ledge fronts. Migration of ledges move away from one edge of a wafer towards the other. The screw pairs situated at the edge of the wafer which is first denuded of ledges would continue to provide the necessary initiation sites for lateral growth across the surface. The important ledge source would be provided by the screw dislocation pairs at that growing surface edge. Screw dislocation pairs which provide non-polar ledges would not affect the epitaxy growth. In any case, nucleation on the epitaxy surface during growth would not be required, as ledges are constantly generated at the wafer edge to provide the sites for continuing lateral growth.

VIII. CONCLUSION

For the first time, reproducible, device quality (110) GaAs/GaAs epitaxy, MESFET devices, and AlGaAs/GaAs quantum wells have been grown by molecular beam epitaxy. The study of facet geometry and chemical nature has shown them to align along the [001] with exposed sides of (100) and (010) and a back plane of $(11\bar{1})$Ga. A thorough characterization of the faceted and non-faceted (110) GaAs epitaxy by microscopy, electrical, optical and chemical methods was necessary to fully understand the facet geometry and initial facet development. This systematic approach to defect analysis has led to the consistent growth of non-faceted (110) GaAs which represents a breakthrough in MBE technology.

Experiments have supported the facet elimination model based on the non-polar (110) GaAs surface and the exposure of Ga and As ledges. Only provision of Ga rich ledges leads to a two dimensional MBE growth resulting in a smooth epitaxy with excellent electrical and optical properties. It is the angling of the GaAs substrate towards the $(11\bar{1})$Ga which results in the exposure of the Ga ledges. The crystalline quality of the epitaxy is shown by the high electron mobility in the (110) GaAs when compared with the (100) GaAs standard. The excellent near-bandgap photoluminescence of the non-faceted (110) GaAs when compared with the (100) standard also supports the device capability of the (110) epitaxy. The low deep level concentrations are further confirmed by DLTS measurements. The CV and IV characteristics exhibit the excellent doping control in the non-faceted (110) films.

The successful results of this investigation also have allowed the growth of a (110) AlGaAs/GaAs superlattice structure whose Al mole fraction was consistent with that of the (100) standard. This is the first AlGaAs-GaAs/GaAs superlattice structure of a (110) orientation and affords the opportunity for fundamental studies of (110) two dimensional electron gas structures as well as AlGaAs-GaAs/GaAs device behavior. The unique properties of (110) GaAs can now be taken full advantage of with both growth and design of GaAs material and devices.

Growth of GaAs/(110)Si is a viable alternative that has yet to be explored due to the previously unattainable high quality growth of (110) GaAs. MBE offers graded index capabilities which have proven helpful in overcoming differences in temperature dependent lattice constants of substrate/epitaxy materials, and the results of this thesis are promising for high quality (110) GaAs material growth without the associated sheet charge from polar face epitaxy.

Finally, an interesting possibility is provided by the CLEFT process referenced in the introduction. If low cost solar cells can be fabricated by taking advantage of the natural (110) cleavage plane of GaAs substrates, then perhaps a high quality epitaxy may be cleaved from the substrate in the same manner to provide lower cost GaAs/AlGaAs epitaxy for certain purposes.

Most importantly, this successful result of device quality (110) GaAs grown by MBE has provided the basis for challenging future materials and device studies. The possibilities of the various (110)

GaAs fundamental studies and material applications are exciting ones, and the achievement of device quality (110) GaAs grown by MBE is only the first step.

APPENDIX I: SCANNING ELECTRON MICROSCOPY TILTING FORMULA

Looking down on a facet:

Define:

θ = angle of known tilt

X = actual width of facet plane observed = unknown

X', X'' = measured width of facet plane (1) or (2)

ϕ = unknown angle of facet from (110) surface

From the drawing below:

$\psi = (\theta - \phi)$

$X' = X \cos(\psi) = X \cos(\theta - \phi)$, which appears larger with clockwise tilting

$X'' = X \cos(\theta + \phi)$, which appears smaller with clockwise tilting

Therefore:

$$X = \frac{X'}{\cos(\theta - \phi)} = \frac{X''}{\cos(\theta + \phi)}$$

and:

$$\frac{X''}{X'} = \frac{\cos(\theta + \phi)}{\cos(\theta - \phi)} , \quad \text{where} \quad \frac{X''}{X'} = R.$$

Utilizing the identy: $\cos(X \pm Y) = \cos X \cos Y \mp \sin X \sin Y$, then

$$R = \frac{\cos(\theta) \cos(\phi) - \sin(\theta) \sin(\phi)}{\cos(\theta) \cos(\phi) + \sin(\theta) \sin(\phi)} .$$

Divide through by $\cos(\theta) \cos(\phi)$, and

$$R = \frac{1 - \tan(\theta) \tan(\phi)}{1 + \tan(\theta) \tan(\phi)}$$

or:

$$R + R \tan(\theta) \tan(\phi) = 1 - \tan(\theta) \tan(\phi)$$

or:

$$1 - R = \tan(\theta) \tan(\phi) [(1+R)]$$

or:

$$(1 - R)/\tan(\theta) [1+R] = \tan(\phi)$$

Since θ is controlled by the SEM operator, and R is measured width of facets, then (ϕ) can be solved for and is the angle of the facet incline from the (110) surface. The actual plane can be found from a stereographic projection.

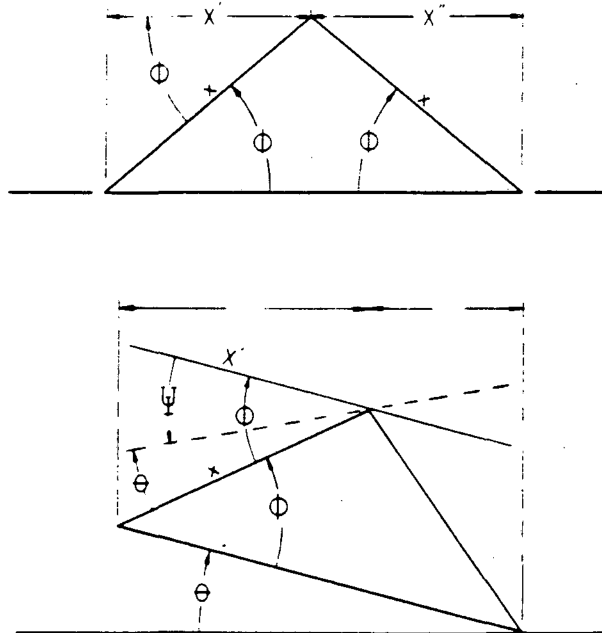

APPENDIX II: TEM PLAN-VIEW AND CROSS-SECTION TECHNIQUE

Plan-View

1) Grind out 3mm discs specimens from sample while white waxed onto glass slide.
2) Remove, and mount 3mm disc onto support. Sand paper down to 100 mil.
3) Dimple and polish exposed side using 1 micron particle size diamond paste and then a cyton polish.
4) Turn specimen onto other side, and dimple and polish down to 25-30 mil.
5) Ar ion mill until thinned.

Cross-Section

1) Cut sample into rectangles of 2.0 x 2.5 mm using diamond saw
2) Silver epoxy faces of rectangles together and heat set over 150°C until dry.
3) Mount several pairs onto stainless steel disc with glue and place in pressure mold with Bakelite enough to cover tops of pairs. Cure bakelite until hardened.
4) Remove from mold and core drill 3mm discs, making sure pairs are centered in core.
5) Mount onto stainless steel supports and proceed from No. 2 of plan-view instructions.

For detailed description of a chemical thinning technique for cross-sectional samples see: S.N.G. Chu and T.T. Sheng, J. Electrochem. Soc., 131, 2263 (1984).

APPENDIX III: GaAs LITHOGRAPHY FOR DLTS

1) GaAs was cleaned in HCl to get rid of In backing.
2) After applying a photoresist, mask I provided the ohmic contact areas.
3) The photoresist and mask I were exposed and developed.
4) Au-Ge evaporation (0.15 microns)
5) Lift-off in acetone removed the photoresist
6) Anneal at 450°C for 40 sec. to provide the ohmic contact
7) Apply photoresist again
8) Mask II to define areas of Schottkey contacts
9) Expose and develop photoresist
10) Au evaporation for Schottkey contacts
11) Lift off photoresist on acetone
12) The final result is a large ohmic contact area with isolated and various size squares of Schottkey contacts. The Schottkey contacts are separated from the ohmic contacts by a bare GaAs border area of ~100 microns.

APPENDIX 4: FCC (110) STEREOGRAPHIC PROJECTION

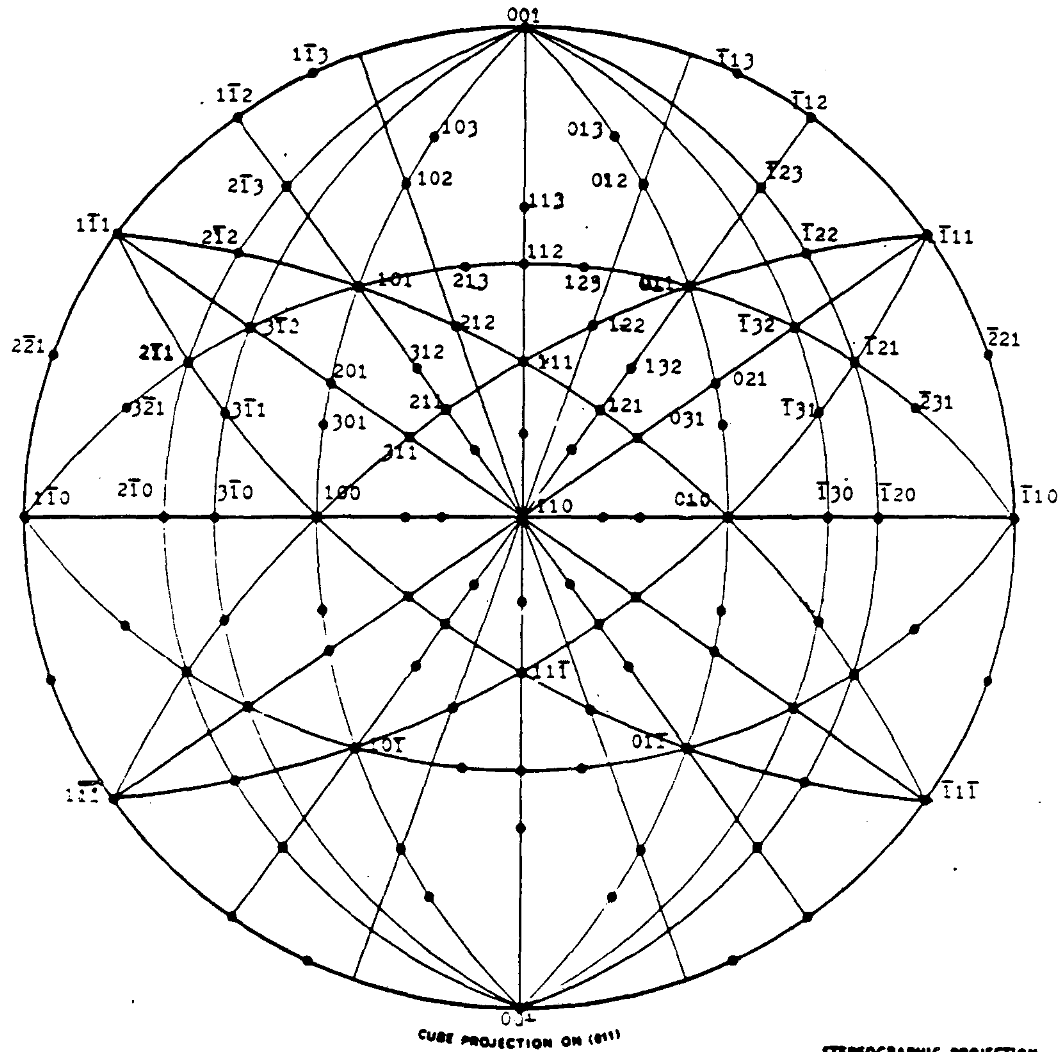

STEREOGRAPHIC PROJECTION
P 317
Published by
POLARON INSTRUMENTS LIMITED
Delviljem House,
4 Shakespeare Road, Finchley, London, N
01-349 9241

REFERENCES

1. A.Y. Cho and J.R. Arthur, Prog. in Sol. State Chem., **10**, 157 (1975).
2. J.C. Bean, "Growth of Doped Silicon Layers by Molecular Beam Epitaxy," in **Impurity Doping Processes in Silicon**, F.F.Y. Wang, ed., (North Holland Publishers, 1981), Chapter 4.
3. P. Skeath, I. Landau, C.Y. Su, and W.E. Spicer, J. Vac. Sci. Technol., **19**, 556 (1981).
4. S.Y. Tong, W.N. Mei, and G. Xu, J. Vac. Sci. Technol., **B2**, 393 (1984).
5. Thomas P. Pearsall and L.C.R. Thomson, Sol. State Elec., **21**, 297 (1978).
6. F. Capasso, T.P. Pearsall, K.K. Thornber, R.E. Nahory, M.A. Pollack, G.B. Bachelet, and J.R. Chelikowsky, J. Appl. Phys., **53**, 3324 (1982).
7. K. Hess, J.Y. Tang, K. Brennan, H. Shichijo, and G.E. Stillman, J. Appl. Phys., **53**, 3327 (1982).
8. Fukunobu Osaka, Yutaka Kishi, Masahiro Kobayashi, and Takashi Mikawa, Appl. Phys. Lett. **47**, 865 (1985).
9. J. McKenna and F.K. Reinhart, J. of App. Phys., **47**, 2069 (1976).
10. J.J. Berenz, J. Kinoshita, T.L. Hierl, and C.A. Lee, Electron. Lett., **15**, 150 (1979).
11. Herbert Kroemer, in "Heteroepitaxy on Silicon," J.C.C. Fan and J.M. Poate, eds., Materials Research Society Symposia Proceedings, **67**, (Pittsburgh, PA, 1986), p. 3.

12. Chin-An Chang, App. Phys. Lett., **40**, 1037 (1982).

13. P. Kruger and J. Pollman, J. Vac. Sci. Technol., **B2**, 415 (1984).

14. R.W. McClelland, C.O. Bazler, and J.C.C. Fan, Appl. Phys. Lett., **37**, 560 (1980).

15. K.L. McLaughlin and M.S. Birrittella, Appl. Phys. Lett., **44** 252 (1984).

16. W.I. Wang, J. Vac. Sci. Technol., **B1**, 630, July-Sept 1983.

17. J.M. Ballingall and C.E.C. Wood, Appl. Phys. Lett., **41**, 947 (1982).

18. L.T. Parechanian, E.R. Weber, and T.L. Hierl, in "Microscopic Identification of Electronic Defects in Semiconductors", N.M. Johnson, S.G. Bishop, G.D. Watkins, eds. Materials Research Society Symposia Proceedings, **46**, (Pittsburgh, PA, 1985), p.391.

19. A.J.W. Moore, "Thermal Faceting," in **Metal Surfaces**, American Society for Metals, (Cleveland, OH, 1963).

20. M. Hillert, Met. Trans. A, **6A**, 5 (1975).

21. J.M. Blakeley, **Introduction to the Properties of Crystal Surfaces**, International Series on Materials Science and Technology, **12**, (Pergamon Press, NY, 1973), p.10.

22. D.A. Porter and K.E. Easterling, **Phase Transformations in Metals and Alloys**, (Van Nostrand Reinhold [UK] Co. Ltd., 1982), p.110.

23. Z. Liliental-Weber and L. Parechanian-Allen, Appl. Phys. Lett., **49**, 1190, (1986).

24. L. Parechanian-Allen, E.R. Weber, J. Washburn, Y.C. Pao, and G. Elliot, submitted to J. Cryst. Growth.

25. L. Parechanian-Allen, E.R. Weber, J. Washburn, and Y.C. Pao in "Characterization of Defects in Materials," R.W. Siegel, R. Sinclair, and J.R. Weertman, eds. Materials Research Society Symposia Proceedings, **82** (Pittsburgh, PA, 1987), in print.

26. T. Murotani, T. Shimanoe, and S. Mitsui, J. Cryst. Growth, **45**, 302 (1978).

27. Vanzetti Systems, c/o Instrument Laboratory, 1323 West 130th St., Gardenia, CA 90247.

28. J. Tafto and J.C.H. Spence, J. Appl. Cryst. **15**, 60 (1982).

29. B.F. Buston, J.A. Eades, J.W. Steeds, and G.M. Rackham, Philos. Trans. R. Soc. London, **281**, 171 (1976).

30. O. Johari and G. Thomas, **The Stereographic Projection and Its Applications** (Interscience Publishers, NY, 1969).

31. L. Jansson, V. Kumar, L.A. Ledebo, and K. Nideborn, J. Phys. E., **14**, 464 (1982).

32. W. Walukiewicz, L. Lagowski, M. Lichensteiger, and H.C. Gatos, J. Appl. Phys., **50**, 899 (1979).

33. R.J. Almassy, D.C. Reynolds, C.W. Litton, and G.L. McCoy, **GaAs and Related Compounds**, (Inst. of Phys. Conf. Ser.) 45, 190 (1979).

34. H. Kunzel and K. Ploog, Appl. Phys. Lett. **37**, 416 (1980).

35. T. Tadaki and K. Shimizu, Trans. Japanese Int. Met., 11, 44 (1970).

36. J.W. Steeds, "Convergent Beam Electron Diffraction," in **Introduction to Analytical Electron Microscopy**, J.J. Hren, J.L. Goldstein, and D.C. Joy, eds., (Plenum Press, NY, 1979), p. 387.

37. Z. Liliental and K. Ishizuka, in **40th Annual Proc. of the Electron Microscopy Society of America 1982**, G.W. Bailey, ed., (Claitor's, Baton Rouge, 1982), p. 448.

38. Mark E. Greiner and Jim Gibbons, J. Appl. Phys., **12**, 5181 (1985).

39. F.A. Ponce, D.K. Biegelsen, J.C. Tramontana, and A.J. Smith, **Proceedings of the 14th International Conference on Defects in Semiconductors**, (Paris, August 18-22, 1986) J.C. Bourgoin and M. Lanoo, eds., in print.

40. F.A. Ponce, W. Stutius, and J.G. Werthen, Thin Solid Films, **104**, 133 (1983).

41. E.R. Weber, H. Ennen, U. Kaufmann, J. Windscheif, J. Schneider, and T. Wosinski, J. Appl. Phys. **53**, 6140 (1982).

42. B. Fischer and H.J. Stoltz, Appl Phys. Lett., **40**, 56 (1982).

43. Dr. Robert Street, Xerox Corporation, Palo Alto, CA, personal conversation.

44. Ya Li Sun, W.T. Masselink, R. Fischer, M.V. Klein, and H. Morkoc, J. Appl. Phys. **55**, 3354 (1984).

45. W.T. Tsang and V. Swaminathan, Appl. Phys. Lett., **39**, 486 (1981).

46. L.J. Brillson, G. Margaritondo, N.G. Stoffel, R.S. Bauer, R.Z. Bachrach, and G. Hannsson, J. Vac. Sci. Technol., 17, 880 (1980).

47. R.Y. DeJule, M.A. Haase, J.E. Stillman, S.C. Palmateer, and J.C.M. Huang, J. Appl. Phys., **57**, 5287 (1985).

48. A. Kahn, J. Vac. Sci. Technol., **A1**, 684 (1983).

49. M. Drosd, Ph.D. Thesis, University of California at Berkeley, (T7,.6, D7873, ENGI), U.C.B. Library.

50. Brian R. Pamplin, ed., **CRYSTAL GROWTH**, (Pergamon Press, Oxford, NY, 1975).

51. J.R. Arthur, Surface Sci. **43**, 449 (1974).

52. J.H. Neave and B.A. Joyce, Journal of Crystal Growth, **44**, 387 (1978).

53. A.Y. Cho, J. Appl. Phys., **47**, 2841 (1976).

54. R.D. Brigans, Phys. Rev. Lett., **56**, 520 (1986).

This report was done with support from the Department of Energy. Any conclusions or opinions expressed in this report represent solely those of the author(s) and not necessarily those of The Regents of the University of California, the Lawrence Berkeley Laboratory or the Department of Energy.

Reference to a company or product name does not imply approval or recommendation of the product by the University of California or the U.S. Department of Energy to the exclusion of others that may be suitable.

LAWRENCE BERKELEY LABORATORY
TECHNICAL INFORMATION DEPARTMENT
UNIVERSITY OF CALIFORNIA
BERKELEY, CALIFORNIA 94720